



**Consecutive Thermal H₂ and Light-Induced O₂
Evolution from Water Promoted by a Metal Complex**

Stephan W. Kohl, *et al.*
Science **324**, 74 (2009);
DOI: 10.1126/science.1168600

**The following resources related to this article are available online at
www.sciencemag.org (this information is current as of April 7, 2009):**

Updated information and services, including high-resolution figures, can be found in the online version of this article at:

<http://www.sciencemag.org/cgi/content/full/324/5923/74>

Supporting Online Material can be found at:

<http://www.sciencemag.org/cgi/content/full/324/5923/74/DC1>

A list of selected additional articles on the Science Web sites **related to this article** can be found at:

<http://www.sciencemag.org/cgi/content/full/324/5923/74#related-content>

This article **cites 29 articles**, 4 of which can be accessed for free:

<http://www.sciencemag.org/cgi/content/full/324/5923/74#otherarticles>

This article appears in the following **subject collections**:

Chemistry

<http://www.sciencemag.org/cgi/collection/chemistry>

Information about obtaining **reprints** of this article or about obtaining **permission to reproduce this article** in whole or in part can be found at:

<http://www.sciencemag.org/about/permissions.dtl>

but creates increased mass transport losses at current densities of $>0.1 \text{ A cm}^{-2}$. It is clear from these results that improvements in electrode mass transport properties are required to overcome this performance loss.

The results of 100-hour durability tests in fuel cells using hydrogen/oxygen and hydrogen/air as anode/cathode gases are shown in fig. S4. Relative to the stable current densities obtained by Bashyam and Zelenay (32) for tests performed under the same conditions (0.2 A cm^{-2} with H_2/O_2 at 0.5 V; 0.13 to 0.14 A cm^{-2} with H_2/air at 0.4 V), the initial current densities produced by the catalyst in this work (0.75 A cm^{-2} with H_2/O_2 at 0.5 V; 0.58 A cm^{-2} with H_2/air at 0.4 V) were much higher and remained higher throughout the 100-hour period, with final values of 0.33 A cm^{-2} with H_2/O_2 at 0.5 V and 0.36 A cm^{-2} with H_2/air at 0.4 V.

The best NPMC in this work has a much higher initial activity, but less stability, than those prepared by Bashyam and Zelenay according to a nonpyrolytic method based on a cobalt salt and polypyrrole deposited on carbon black (32). Continued research must now focus on improving the stability of these NPMCs and optimizing their cathode mass-transport properties.

References and Notes

- H. A. Gasteiger, S. S. Kocha, B. Sompalli, F. T. Wagner, *Appl. Catal. B* **56**, 9 (2005).
- H. A. Gasteiger, J. E. Panels, S. G. Yan, *J. Power Sources* **127**, 162 (2004).

- R. Jasinski, *Nature* **201**, 1212 (1964).
- J. P. Dodelet, in *N4-Macrocyclic Metal Complexes*, J. H. Zagal, F. Bedioui, J. P. Dodelet, Eds. (Springer, New York, 2006), pp. 83–147.
- S. Gupta, D. Tryk, I. Bae, W. Aldred, E. Yeager, *J. Appl. Electrochem.* **19**, 19 (1989).
- M. Yuasa et al., *Chem. Mater.* **17**, 4278 (2005).
- N. P. Subramanian et al., *J. Power Sources* **157**, 56 (2006).
- E. B. Easton, A. Bonakdarpour, J. R. Dahn, *Electrochem. Solid State Lett.* **9**, A463 (2006).
- R. Z. Yang, A. Bonakdarpour, E. B. Easton, P. Stoffyn-Egli, J. R. Dahn, *J. Electrochem. Soc.* **154**, A275 (2007).
- J. Maruyama, I. Abe, *Chem. Commun.* **2007**, 2879 (2007).
- T. E. Wood, Z. Tan, A. K. Schmoekel, D. O'Neill, R. Atanasoski, *J. Power Sources* **178**, 510 (2008).
- A. Garsuch, K. MacIntyre, X. Michaud, D. A. Stevens, J. R. Dahn, *J. Electrochem. Soc.* **155**, B953 (2008).
- T. Schilling, M. Bron, *Electrochim. Acta* **53**, 5379 (2008).
- A. H. C. Sirk, S. A. Campbell, V. I. Birss, *J. Electrochem. Soc.* **155**, B592 (2008).
- J. Maruyama, N. Fukui, M. Kawaguchi, I. Abe, *J. Power Sources* **182**, 489 (2008).
- V. Nallathambi, J.-W. Lee, S. P. Kumaraguru, G. Wu, B. N. Popov, *J. Power Sources* **183**, 34 (2008).
- U. I. Koslowski, I. Abs-Wurmbach, S. Fiechter, P. Bogdanoff, *J. Phys. Chem. C* **112**, 15356 (2008).
- J. Maruyama, J. Okamura, K. Miyazaki, Y. Uchimoto, I. Abe, *J. Phys. Chem. C* **112**, 2784 (2008).
- J. M. Ziegelbauer et al., *J. Phys. Chem. C* **112**, 8839 (2008).
- F. Jaouen, F. Charreter, J. P. Dodelet, *J. Electrochem. Soc.* **153**, A689 (2006).
- F. Jaouen, M. Lefèvre, J. P. Dodelet, M. Cai, *J. Phys. Chem. B* **110**, 5553 (2006).
- F. Jaouen, J. P. Dodelet, *J. Phys. Chem. C* **111**, 5963 (2007).
- F. Jaouen, A. M. Serventi, M. Lefèvre, J. P. Dodelet, P. Bertrand, *J. Phys. Chem. C* **111**, 5971 (2007).
- F. Jaouen, S. Marquette, J. P. Dodelet, G. Lindbergh, *J. Phys. Chem. B* **107**, 1376 (2003).
- F. Charreter, F. Jaouen, S. Ruggeri, J. P. Dodelet, *Electrochim. Acta* **53**, 2925 (2008).
- See supporting material on Science Online.
- U. S. Department of Energy, Technical Plan: Fuel Cells, 2007 (www1.eere.energy.gov/hydrogenandfuelcells/mypp/pdfs/fuel_cells.pdf).
- F. Charreter, S. Ruggeri, F. Jaouen, J. P. Dodelet, *Electrochim. Acta* **53**, 6881 (2008).
- F. Jaouen, J. P. Dodelet, *Electrochim. Acta* **52**, 5975 (2007).
- M. Lefèvre, J.-P. Dodelet, *Electrochim. Acta* **53**, 8269 (2008).
- Although detailed cost analysis of these Fe-based electrocatalysts was not performed, their principal elements are carbon, nitrogen, and iron and they require no expensive precursors or processing steps. Their manufacturing cost is conservatively estimated to be at least two orders of magnitude lower than that of current Pt-based ORR catalysts for PEMFCs.
- R. Bashyam, P. Zelenay, *Nature* **443**, 63 (2006).
- Supported by General Motors of Canada and the Natural Sciences and Engineering Council of Canada. The Cabot Corporation provided the carbon black. U.S. patent application US 61/112,844 related to this work was filed on 10 November 2008.

Supporting Online Material

www.sciencemag.org/cgi/content/full/324/5923/71/DC1

Materials and Methods

SOM Text

Figs. S1 to S4

Tables S1 and S2

References

19 December 2008; accepted 9 February 2009

10.1126/science.1170051

Consecutive Thermal H_2 and Light-Induced O_2 Evolution from Water Promoted by a Metal Complex

Stephan W. Kohl,¹ Lev Weiner,² Leonid Schwartsburd,¹ Leonid Konstantinovski,² Linda J. W. Shimon,² Yehoshoa Ben-David,¹ Mark A. Iron,² David Milstein^{1*}

Discovery of an efficient artificial catalyst for the sunlight-driven splitting of water into dioxygen and dihydrogen is a major goal of renewable energy research. We describe a solution-phase reaction scheme that leads to the stoichiometric liberation of dihydrogen and dioxygen in consecutive thermal- and light-driven steps mediated by mononuclear, well-defined ruthenium complexes. The initial reaction of water at 25°C with a deaeromatized ruthenium (II) [Ru(II)] pincer complex yields a monomeric aromatic Ru(II) hydrido-hydroxo complex that, on further reaction with water at 100°C, releases H_2 and forms a cis dihydroxo complex. Irradiation of this complex in the 320-to-420-nanometer range liberates oxygen and regenerates the starting hydrido-hydroxo Ru(II) complex, probably by elimination of hydrogen peroxide, which rapidly disproportionates. Isotopic labeling experiments with H_2^{17}O and H_2^{18}O show unequivocally that the process of oxygen–oxygen bond formation is intramolecular, establishing a previously elusive fundamental step toward dioxygen-generating homogeneous catalysis.

The design of efficient catalytic systems for splitting water into H_2 and O_2 , driven by sunlight without the use of sacrificial reductants or oxidants, is among the most important challenges facing science today, under-

pinning the long-term potential of hydrogen as a clean, sustainable fuel (1, 2). In this context, it is essential to enhance our basic understanding of the fundamental chemical steps involved in such processes (3–17). Of the two parts of the water-

splitting cycle, the oxidation half-cycle to form O_2 presents the greatest challenge. Well-defined metal complexes that catalyze water oxidation to dioxygen are rare and generally require a sacrificial strong oxidant. The molecular mechanisms of such systems, including that of the intensively studied “blue dimer” $\text{cis,cis-}[(\text{bpy})_2(\text{H}_2\text{O})\text{Ru}^{\text{III}}\text{ORu}^{\text{III}}(\text{OH}_2)(\text{bpy})_2]^{4+}$ (3, 11, 12), are generally thought to involve metal oxo intermediates and bimolecular steps, but clarification of the fundamental chemical principles responsible for O–O bond formation remains a considerable challenge. In addition, a major challenge faced by hydrogen and oxygen photogeneration systems based on soluble metal complexes is that for a viable system, the two half-cycles must be combined, avoiding the use of sacrificial oxidants and reductants. We present here a ruthenium-mediated reaction sequence that, in a stepwise stoichiometric manner, generates hydrogen thermally and oxygen photochemically, involves well-defined complexes, and demonstrates the feasibility of unimolecular O–O bond formation at a single metal center.

¹Department of Organic Chemistry, The Weizmann Institute of Science, Rehovot 76100, Israel. ²Department of Chemical Research Support, The Weizmann Institute of Science, Rehovot 76100, Israel.

*To whom correspondence should be addressed. E-mail: david.milstein@weizmann.ac.il

We have previously reported that the non-aromatic pincer Ru(II) complex **1** (Fig. 1) is a powerful catalyst for the coupling of alcohols to form esters with the liberation of H₂ (*18*) and for the dehydrogenative coupling of alcohols with amines to produce amides (*19*). We have now studied the reactivity of this complex with water. The addition of one equivalent of water to a solution of **1** in tetrahydrofuran (THF) at room temperature immediately led to ligand aromatization with quantitative formation of the *trans* hydrido-hydroxo complex **2** (Fig. 1),

which we isolated and fully characterized (*20*). This compound is probably formed by a mechanism involving coordination of water at the vacant coordination site *trans* to the hydride ligand, followed by proton migration to the side arm. This unique water activation process involves cooperation between the metal and the ligand and no change in the metal oxidation state (*21*).

Characteristic spectroscopic features in the ¹H nuclear magnetic resonance (NMR) spectrum of **2** are the large downfield shift of the

hydride ligand resonance from -26.5 parts per million (ppm) (d, ²J_{PH} = 25.5 Hz) in **1** to -14.9 ppm (d, ²J_{PH} = 27.5 Hz) and a doublet at -1.4 ppm (³J_{PH} = 2.3 Hz) assigned to the hydroxo ligand. If one equivalent of D₂O is used instead of H₂O, one deuterium atom is incorporated at the side-arm benzylic carbon, leading to a broad peak (because of unresolved small ²J_{HD} and ²J_{PD}) at 2.8 ppm in the ²H NMR spectrum; the OD group gives rise to a signal at -1.2 ppm (complex **2-D₂**, Fig. 1). These reactions are reversible. Placing the solid under vacuum or heating it in benzene solution at 65°C resulted in water elimination to quantitatively yield the starting complex **1**. Direct spectroscopic evidence for coordination of the hydroxo group to the metal center was obtained by adding one equivalent of H₂¹⁷O to **1** in THF. The oxygen atom in the labeled complex **2-¹⁷O** exhibits a singlet at 32.43 ppm in the ¹⁷O NMR spectrum (in THF). Coupling (²J_{OP}, ²J_{OC}) of the ¹⁷O atom (s = 5/2) with the adjacent ligands leads to broadening of the signal in the ³¹P NMR spectrum at 112.14 ppm and the appearance of a more complicated signal for the carbonyl ligand in the ¹³C{¹H}NMR spectrum (δ = 209.27 ppm). The doublet in the ¹H NMR spectrum (δ = 14.78 ppm) assigned to the hydride ligand in the *trans* position is not affected.

Repeating the reaction in benzene by adding an excess of water to **1** resulted in formation of colorless crystals at the interface between the water and benzene layers. X-ray diffraction analysis of the isolated solid (**2.nH₂O**) shows a distorted octahedral coordination geometry at ruthenium (Fig. 2). The Ru–O–H non-linear angle [103(3)] indicates repulsion between the oxygen lone pairs and d electrons of the complex (22, 23). The crystals are composed of alternating layers of the metal complex, benzene, and water. The hydroxo groups of the complex are involved in hydrogen bonding with the water layer (figs. S4 to S6). These crystals are stable below 10°C and release the solvated water at room temperature.

Heating complex **2** (or **2.nH₂O**) in refluxing water for 3 days resulted in evolution of H₂ with concomitant formation of the green *cis* dihydroxo complex **3** (Fig. 3). The gas was collected in a burette, and hydrogen was detected by the reaction of the gas phase with (PEt₃)₃IrCl to form *mer-cis*-(PEt₃)₃Ir(H)₂Cl (*24*). H₂ was quantified with gas chromatography (GC) (yield: 37%). The NMR yield of the complex **3** was 45%. Some unreacted **2.nH₂O** (25%) remained, the rest being unidentified products. This reaction may proceed by electrophilic attack by water on the hydride ligand. Pure **3** was independently prepared by reaction of **2.nH₂O** with N₂O (*25*, *26*): N₂O was bubbled into a THF solution of **2.nH₂O** for 10 min at room temperature, after which the solution was stirred overnight and turned green. We isolated and fully characterized the result-

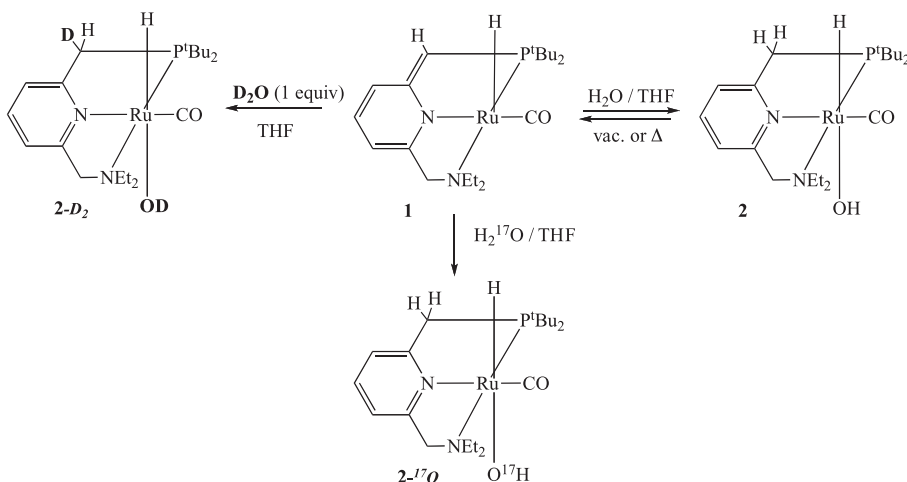


Fig. 1. Reactions of water with complex **1**. Et, ethyl.

Fig. 2. Structure of the *trans* hydrido-hydroxo complex **2.nH₂O** (ellipsoids shown at 50% probability level). Hydrogen atoms are shown only for the hydride and hydroxo ligands. The water and benzene layers are omitted for clarity. Selected bond distances (in angstroms) and angles (in degrees): Ru1–H1, 1.54(3); Ru1–C1, 1.820(3); Ru1–N2, 2.097(2); Ru1–N1, 2.241(2); Ru1–O2, 2.261(2); Ru1–P1, 2.2653(8); N2–Ru1–C1, 173.02(10); N1–Ru1–P1, 159.12(7); H1–Ru1–O2, 171.9(13); N2–Ru1–O2, 86.94(8); N1–Ru1–O2, 82.44(9); Ru1–O2–H2, 103(3).

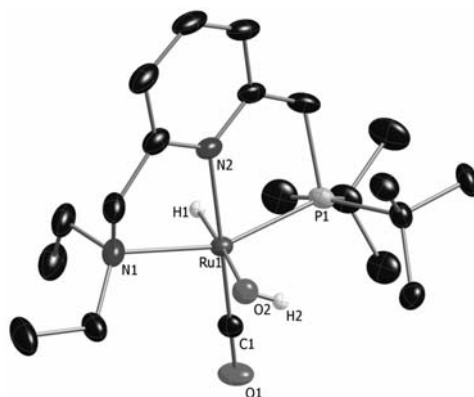


Fig. 3. Thermal activation of water by the hydrido-hydroxo complex **2** with liberation of H₂, independent synthesis of the dihydroxo complex **3** using N₂O, and O₂ formation upon photolysis of **3** regenerating complex **2**. *h*, Planck's constant; *v*, frequency.

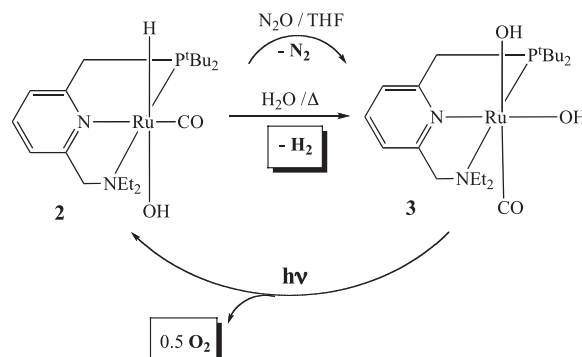


Fig. 4. Photolysis of isotopically labeled dihydroxo complexes. (A) Synthesis and photolysis of complexes **3-¹⁸O¹⁸O** and **3-¹⁸O¹⁶O**. (B) Mass spectrum of a gaseous extract from the photolytic reaction of equimolar amounts of **3-¹⁸O¹⁸O** and **3-¹⁶O¹⁶O**, showing virtually no cross-over.

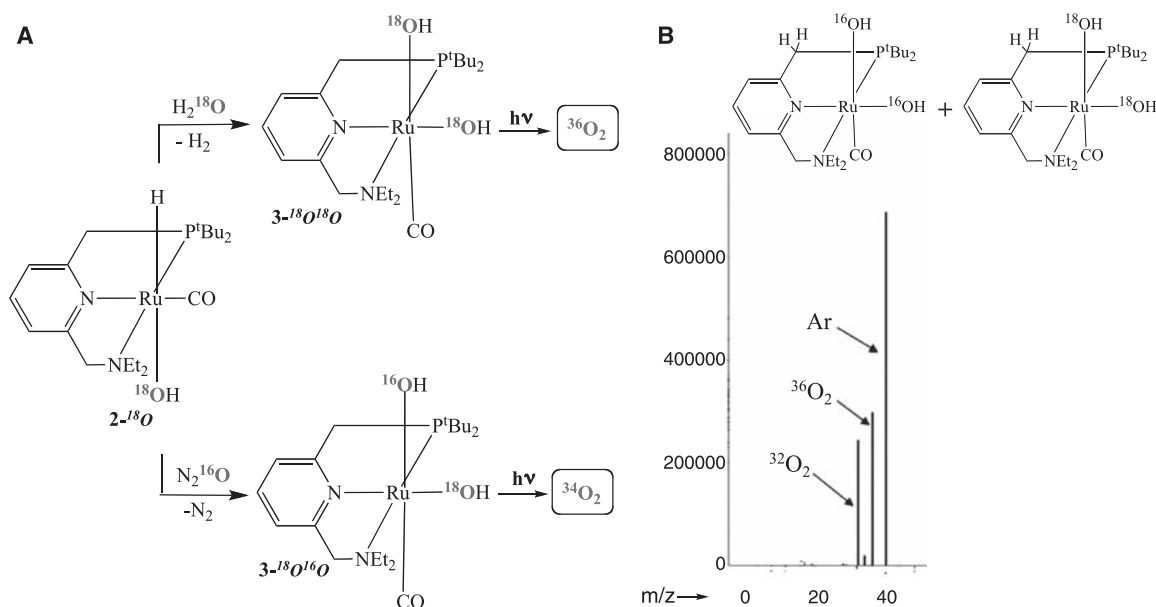
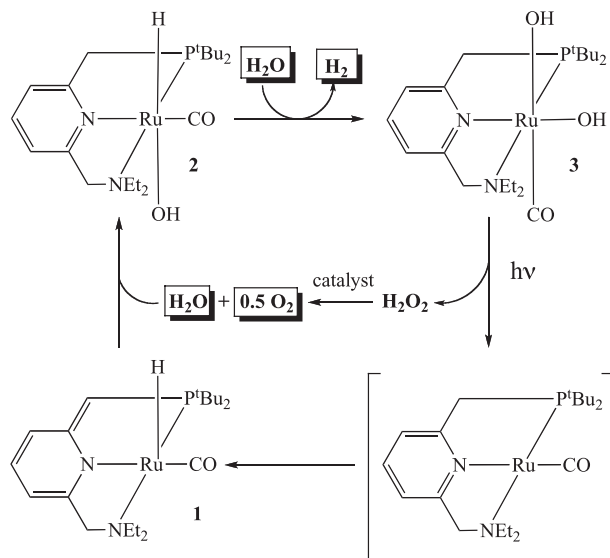


Fig. 5. Proposed mechanism for the formation of H₂ and O₂ from water.



ant green microcrystalline solid **3** (60% yield). It is stable in a THF solution up to 65°C but decomposes into unidentified products at 102°C in dioxane. The ³¹P{¹H} NMR spectrum of **3** shows a singlet at 94.0 ppm, representing an upfield shift of 14 ppm relative to the corresponding singlet of complex **2**. The two tert-butyl (^tBu) groups of P^tBu₂ give rise to different signals in both the ¹H and ¹³C{¹H} NMR spectra, and the ethyl groups of NEt₂ are also non-equivalent, indicating C₁ symmetry and a cis dihydroxo arrangement. The hydroxo ligands give rise to a broad signal at -7.4 ppm in the ¹H NMR spectrum and absorb at 3413 cm⁻¹ in the infrared (IR) spectrum. The carbonyl ligand exhibits a doublet at 207.4 ppm (²J_{PC} = 16.1 Hz) in the ¹³C{¹H} NMR spectrum and absorbs at 1923 cm⁻¹ in the IR spectrum. The main peak in the mass spectrum (electrospray ionization)

at mass/charge ratio (m/z) = 453 (100) can be assigned to the cation [M - OOH]⁺ and the peak at m/z = 469 (18) is characteristic for [M - OH]⁺. Elemental analysis agrees with the calculated values for our posited structure.

We next studied the stability of complex **3** on exposure to light. Irradiation of THF or aqueous solutions of **3** under N₂ or Ar with a 300-W halogen lamp filtered through perspex (27) over 2 days resulted in a color change from green to greenish-yellow, accompanied by O₂ evolution. NMR of the solution showed that besides unreacted **3** (33%), the hydrido-hydroxo complex **2.nH₂O** (45%) was formed, in addition to some unidentified by-products (22%), most probably phosphine oxides (Fig. 3). The liberated gas was identified as dioxygen by GC-mass spectrometry (GC-MS) and by the reaction with (PEt₃)₃IrCl to form the dioxy-

gen complex (PEt₃)₃Ir(O₂)Cl (**20**). This specific and very sensitive reaction was also used for quantification (**20**). The yield of the detected dioxygen formed from the reaction in water was 23% (34% based on reacted **3**). When irradiation of aqueous solutions of **3** was performed under argon flow to remove the generated O₂, clean conversion of **3** (49%, the rest being unreacted **3**) to **2.nH₂O** (49%) was observed, with no by-products being formed, indicating that the unidentified by-products are a result of reaction with the generated dioxygen.

To verify that O₂ was released from the dihydroxo complex, a labeled complex bearing two ¹⁸OH groups (**3-¹⁸O¹⁸O**) was prepared using H₂¹⁸O (Fig. 4). The ¹⁸O-H stretching vibration is shifted in the IR spectrum to lower energy by 14 wavenumbers, to 3399 cm⁻¹, whereas all NMR spectra are identical to those of **3**. Upon irradiation (27) of **3-¹⁸O¹⁸O** in H₂O, ³⁶O₂ was formed as the major dioxygen product, as confirmed by GC-MS (Fig. 4A and fig. S3A). No exchange between **3-¹⁸O¹⁸O** and H₂¹⁶O was observed, indicating that no substantial Ru-OH dissociation took place.

An important question is whether the O-O bond formation process is intra- or intermolecular. To address this issue, we prepared the isotopically mixed-labeled dihydroxo complex **3-¹⁸O¹⁶O** by treatment of **2-¹⁸O** with N₂¹⁶O (Fig. 4A). Upon photolysis, ³⁴O₂ was formed predominantly with only small amounts of ³²O₂ and ³⁶O₂ observed (observed ratio ³²O₂:³⁴O₂:³⁶O₂, 3.8:16.2:1) (fig S3B) (**20**). Moreover, we performed a crossover experiment involving photolysis of equimolar amounts of complexes **3-¹⁸O¹⁸O** and **3-¹⁶O¹⁶O**, resulting in formation of ³⁶O₂ and ³²O₂ with only a small amount of ³⁴O₂ (observed ratio ³²O₂:³⁴O₂:³⁶O₂, 13.1:1:15.6) (Fig. 4B). Thus, our results unambiguously show that the O-O

bond formation process in this system is intramolecular and involves a single metal center.

We suggest that upon photolysis, complex **3** liberates hydrogen peroxide in a reductive elimination step (28, 29), which then catalytically disproportionates into O₂ and water (Fig. 5). Our labeling studies show that, if H₂O₂ is indeed an intermediate in the O₂ generation process, then O₂ is formed by two electron oxidation of H₂O₂ without scission of the O–O bond, as reported for the reaction catalyzed by the enzyme catalase (30).

The metal-to-ligand charge transfer (MLCT) band of **3** has an absorbance maximum in the ultraviolet-visible (UV-Vis) spectrum in water at wavelength $\lambda = 380$ nm (extinction coefficient $\epsilon = 8157$ cm⁻¹M⁻¹). Weaker absorptions appear at $\lambda = 459$ nm ($\epsilon = 2045$ cm⁻¹M⁻¹) and $\lambda = 716$ nm ($\epsilon = 505$ cm⁻¹M⁻¹) (fig. S2). The theoretical UV-Vis spectrum (of the NMe₂, PMe₂ model of **3**) in water was determined by time-dependent density functional theory (TDDFT) (figs S8 and S9 and table S5). When a 400-nm filter was used, the yield of produced O₂ decreased to only 8 to 10%. Together with filtration of wavelengths of $\lambda < 320$ nm by the perspex filter, this observation is in line with an effective spectral range corresponding to the MLCT band of **3** (320 to 420 nm).

Unlike the dihydroxo complex **3**, the hydrido-hydroxo complex **2** was stable toward irradiation with a 300-W halogen lamp for 2 days, with or without the perspex filter, and did not release O₂. This observation is in line with an intramolecular, mononuclear O–O bond formation mechanism.

Because the intermediacy of H₂O₂ might give rise to hydroxyl radicals, via a Fenton-type reaction (31), we employed the spin trap 5,5-dimethyl-1-pyrroline-1-oxide (DMPO) (32) to detect them. Electron paramagnetic resonance spectra did provide evidence for DMPO-OH adducts (fig. S7A). However, it is clear that these hydroxyl radicals are not substantially involved in O₂ production (as the isotopic labeling experiments would have resulted in scrambling). Thus, in the presence of the OH radical scavenger *tert*-butanol (33), no hydroxyl radicals were observed, whereas the amount of O₂ formed remained unchanged. Further evidence supporting hydrogen peroxide as the source of hydroxyl radicals, and that the hydroxyl radicals are not the source of the produced O₂, was obtained from experiments with the enzyme catalase, which is an extremely efficient catalyst for the disproportionation of hydrogen peroxide to O₂ and water by a non-radical mechanism. If H₂O₂ were the source of hydroxyl radicals, its interception by catalase would retard their formation. When irradiation of **3** was performed in the presence of catalase, only traces of hydroxyl radicals were observed (fig. S7C), whereas the amount of O₂ produced remained almost unchanged (actually slightly increased). Thus, we believe that H₂O₂

forms photolytically from **3** and undergoes disproportionation to O₂ and water, with only a marginal amount of it forming hydroxyl radicals, perhaps by a Fenton-type reaction. As expected, no OH radicals were detected when the hydrido-hydroxo complex **2.nH₂O** was irradiated.

Combining the separate stoichiometric reactions presented here gives rise to a stepwise cycle in which H₂ and O₂ are released in consecutive steps, and the starting Ru complex is regenerated (Fig. 5). The cycle starts with the *trans* hydrido-hydroxo complex **2.nH₂O** that reacts with water under refluxing conditions, evolving H₂ and forming the *cis* dihydroxo complex **3**. The second step is light-induced. Irradiating **3** may release hydrogen peroxide by reductive elimination, probably forming a Ru(0) intermediate, which converts to **1** by migration of a proton from the methylene group of the phosphorus side arm to the ruthenium center to form a hydride ligand with coincident dearomatization of the pyridine ring (34, 35). The liberated hydrogen peroxide is then rapidly catalytically decomposed into dioxygen and water. A possible catalyst for this latter reaction is complex **1**. The addition of a very dilute THF solution of **1** to a THF solution of hydrogen peroxide at room temperature resulted in immediate O₂ evolution, as detected by GC-MS and by reaction with (PEt₃)₃IrCl (20). In the last step of the cycle, the water reacts readily with **1** to form the starting complex **2**.

We believe that our studies indicate a distinct approach toward a complete cycle for the generation of dihydrogen and dioxygen from water catalyzed by metal complexes and show that light-induced O–O bond formation can be intramolecular and need not necessarily involve bimolecular mechanisms, dinuclear complexes, and metal oxo intermediates.

References and Notes

- N. S. Lewis, D. G. Nocera, *Proc. Natl. Acad. Sci. U.S.A.* **103**, 15729 (2006).
- V. Balzani, A. Credi, M. Venturi, *ChemSusChem* **1**, 26 (2008).
- R. A. Binstead, C. W. Chronister, J. Ni, C. W. Hartshorn, T. J. Meyer, *J. Am. Chem. Soc.* **122**, 8464 (2000).
- J. H. Alstrum-Acevedo, M. K. Brennaman, T. J. Meyer, *Inorg. Chem.* **44**, 6802 (2005).
- T. A. Betley, Q. Wu, T. Van Voorhis, D. G. Nocera, *Inorg. Chem.* **47**, 1849 (2008).
- J. K. Hurst, *Coord. Chem. Rev.* **249**, 313 (2005).
- M. Yagi, M. Kaneko, *Chem. Rev.* **101**, 21 (2001).
- W. Ruttiger, G. C. Dismukes, *Chem. Rev.* **97**, 1 (1997).
- I. Romero et al., *Inorg. Chem.* **47**, 1824 (2008).
- Z. Deng, H.-W. Tseng, R. Zong, D. Wang, R. Thummel, *Inorg. Chem.* **47**, 1835 (2008).
- J. K. Hurst, J. L. Cape, A. E. Clark, S. Das, C. Qin, *Inorg. Chem.* **47**, 1753 (2008).
- X. Yang, M.-H. Baik, *J. Am. Chem. Soc.* **128**, 7476 (2006).
- J. T. Muckerman, D. E. Polyansky, T. Wada, K. Tanaka, E. Fujita, *Inorg. Chem.* **47**, 1787 (2008).
- N. D. McDaniel, F. J. Coughlin, L. L. Tinker, S. Bernhardt, *J. Am. Chem. Soc.* **130**, 210 (2008); and references therein.
- V. G. Gletii et al., *Angew. Chem. Int. Ed.* **47**, 3896 (2008); and references therein.
- J. Limburg et al., *Science* **283**, 1524 (1999).
- S. Chakraborty, T. J. Wadas, H. Hester, R. Schmehl, R. Eisenberg, *Inorg. Chem.* **44**, 6865 (2005).
- J. Zhang, G. Leitus, Y. Ben-David, D. Milstein, *J. Am. Chem. Soc.* **127**, 10840 (2005).
- C. Gunanathan, Y. Ben-David, D. Milstein, *Science* **317**, 790 (2007).
- Experimental details are available as supporting material on Science Online.
- DFT calculations on a model system (with PMe₂, NMe₂ groups) at the PCM(H₂O)-M06/SDB-cc-pVDZ/M06/SDD(d) level indicate that the Gibbs free energy change (ΔG) = -5.4 kcal/mol for H₂O coordination and ΔG = -5.7 kcal/mol and ΔG^\ddagger = 9.4 kcal/mol for the subsequent proton migration. Addition of a bridging water molecule as part of the proton-transfer transition state lowers the barrier to ΔG^\ddagger = 3.6 kcal/mol. According to this DFT calculation, the D atom would selectively transfer to the same side of the double bond as the hydroxo ligand, but we have not yet demonstrated this experimentally.
- P. E. M. Siegbahn, M. R. A. Blomberg, M. Svenson, *J. Phys. Chem.* **97**, 2564 (1993).
- D. Milstein, J. C. Calabrese, I. D. Williams, *J. Am. Chem. Soc.* **108**, 6387 (1986).
- O. Blum, D. Milstein, *J. Am. Chem. Soc.* **117**, 4582 (1995).
- Reaction of a Ru(H)(OH) complex with N₂O was reported to yield a Ru(OH)₂ complex (26). We found that bubbling N₂O into a solution of the crystalline material **2.nH₂O** (rather than **2**) avoided the formation of impurities.
- A. W. Kaplan, R. G. Bergman, *Organometallics* **17**, 5072 (1998).
- We used a filter made of polymethylmethacrylate (perspex, thickness = 1 cm) during the irradiation. This material absorbs UV light at wavelengths shorter than $\lambda = 320$ nm. Irradiation without perspex gave more by-products, and dioxygen was formed in only 19% yield.
- Photochemically induced reductive elimination of HOCl from a Pt^(IV)(Cl)(OH) complex was suggested (29).
- Y. Nakabayashi et al., *Chem. Eur. J.* **13**, 3980 (2007).
- S. Kato, T. Ueno, S. Fukuzumi, Y. Watanabe, *J. Biol. Chem.* **279**, 52376 (2004).
- C. Walling, *Acc. Chem. Res.* **8**, 125 (1975).
- M. A. Grela, M. E. J. Coronel, A. J. Colussi, *J. Phys. Chem.* **100**, 16940 (1996).
- J. von Sonntag, E. Mwula, K. Hildenbrand, C. von Sonntag, *Chem. Eur. J.* **10**, 440 (2004).
- For such a proton migration process with a PNP-Ir(III) complex, see (35).
- E. Ben-Ari, G. Leitus, L. J. W. Shimon, D. Milstein, *J. Am. Chem. Soc.* **128**, 15390 (2006).
- This project was supported by the Israel Science Foundation, the Petroleum Research Fund administered by the American Chemical Society, the programme for Deutsch-Israelische Partnerschaft, and the Helen and Martin Kimmel Center for Molecular Design. S.W.K. thanks the Humboldt Foundation for a Feodor Lynen Postdoctoral Fellowship. D.M. holds the Israel Matz Professorial Chair of Organic Chemistry. We thank M. Feller for fruitful discussions, A. Tishbee and R. Kramer for performing mass spectroscopy, A. Khenkin and H. Weissman for carrying out GC-MS and GC measurements, and E. Shirman for photon flux measurements. Structural parameters for **2.nH₂O** are available free of charge from the Cambridge Crystallographic Data Centre under identification number CCDC-681749.

Supporting Online Material

www.sciencemag.org/cgi/content/full/324/5923/74/DC1
Materials and Methods
SOM Text
Figs. S1 to S9
Tables S1 to S5
References

17 November 2008; accepted 13 February 2009
10.1126/science.1168600



Supporting Online Material for

Consecutive Thermal H₂ and Light-Induced O₂ Evolution from Water Promoted by a Metal Complex

Stephan W. Kohl, Lev Weiner, Leonid Schwartsburd, Leonid Konstantinovski, Linda J. W. Shimon, Yehoshoa Ben-David, Mark A. Iron, David Milstein*

*To whom correspondence should be addressed. E-mail: david.milstein@weizmann.ac.il

Published 3 April 2009, *Science* **324**, 74 (2009)
DOI: 10.1126/science.1168600

This PDF file includes:

Materials and Methods
SOM Text
Figs. S1 to S9
Tables S1 to S5
References

Supporting Online Material for

Consecutive Thermal H₂ and Light-Induced O₂ Evolution from Water Promoted by a Metal Complex

Stephan W. Kohl,¹ Lev Weiner,² Leonid Schwartsburd,¹ Leonid
Konstantinovski,² Linda J. W. Shimon,² Yehoshoa Ben-David,¹

Mark A. Iron², David Milstein^{1*}

Department of Organic Chemistry and Unit of Chemical Research Support,
The Weizmann Institute of Science,
Rehovot 76100, Israel

¹ Department of Organic Chemistry

² Unit of Chemical Research Support

Materials and Methods. All experiments with metal complexes and phosphine ligands were carried out under an atmosphere of purified nitrogen in a Vacuum Atmospheres glovebox equipped with a MO 40-2 inert gas purifier or using standard Schlenk techniques under purified nitrogen or argon. All solvents were reagent grade or better. All organic non-deuterated solvents were refluxed over sodium/benzophenone ketyl and distilled under argon atmosphere. Deuterated organic solvents were used as received. All solvents were degassed with argon and organic solvents were kept over 4 Å molecular sieves. The ligand

(2-(di-*tert*-butylphosphino-methyl)-6-diethylaminomethyl)pyridine) (PNN) (*S1*), the complexes (PNN)RuHCl(CO) (*S1*) and **1** (*S1*) the precursor RuHCl(CO)(PPh₃)₃ (*S2*) and (PEt₃)₃IrCl (*S3*) were prepared according to literature procedures. HPLC grade sterile water was used, obtained by treatment of deionized water (purified with an ion-exchange device “Zelion” , Israel) with a Barnstead NANOpure DIamond Water Purification System (Barnstead D11931). H₂¹⁸O (97% enriched) was purchased from Rotem Industries Ltd., Beer Sheva, and H₂¹⁷O (10% enriched) from D-Chem. Ltd., Israel. N₂O was obtained from Gas Technologies, Israel. Catalase from bovine liver was received from Sigma. All other chemicals were used as received (Aldrich) without further purification. ¹H NMR spectra were obtained at 250 MHz (Bruker DPX) or 400 MHz (Bruker “Avance”) or 500 MHz (Bruker “Avance”). ¹³C{¹H} NMR spectra were obtained at 100 MHz or 126 MHz. ³¹P{¹H} NMR spectra were obtained at 101 MHz or 162 MHz or 202 MHz. ²H NMR spectra were obtained at 61 MHz. ¹⁷O NMR spectra were obtained at 68 MHz. ¹H, ²H, ¹³C, ³¹P and ¹⁷O NMR chemical shifts are reported in parts per million downfield from tetramethylsilane and were referenced to residual protiated (¹H) or deuterated solvents (¹³C) or natural abundance deuterated solvent (²H) or enriched D₂¹⁷O (¹⁷O). ³¹P NMR chemical shifts are reported in parts per million downfield from H₃PO₄ and referenced to an external 85% solution of phosphoric acid in D₂O. Abbreviations used in the NMR follow-up experiments: b, broad; s, singlet; d, doublet; t, triplet; q, quartet; m, multiplet; vt, virtual triplet. IR spectra were recorded on a Nicolet FT-IR spectrophotometer. UV/Vis absorption measurements were made on a Varian Cary-5000 UV-Vis-NIR spectrophotometer. Mass spectra were recorded on Micromass Platform LCZ 4000, using Electro Spray Ionization (ESI) mode [conditions: sample dissolved in CH₂Cl₂ solution, added to methanol

(MeOH:CH₂Cl₂ 30:1) and a sample directly infused at 5 μl/min. [Cone Voltage 43 V, Extractor 4V, Source block temp 100 °C, desolvation temp 150 °C]. GC analysis of dihydrogen was achieved on a HP 6890 series system, equipped with a 5 ft. × 1/8 inch stainless steel 45/60 Carboxen 1000 column and a TC detector. GC/MS analysis of dioxygen was performed on a HP 6890 series system, equipped with a 30 m, 5% phenylsiloxane column and a Mass Selective Detector 5973. Elemental analyses were performed at Kolbe Laboratorium, Mülheim a. d. Ruhr, Germany. The irradiation experiments were done using a 300 W halogen lamp. Electron Paramagnetic Resonance (EPR) spectra were recorded on an ELEXSYS 500 spectrometer (Bruker, Germany) in 100 μL quartz capillary. The g-values of the complexes in glassy solutions were determined using 2,2-diphenyl-1-picrylhydrazyl (DPPH) resonance signal (g = 2.0037) as a standard. Enzymatic activity of catalase was assessed by adding the solution of the enzyme in water to a solution of hydrogen peroxide in water. The time-dependent decrease of absorption of hydrogen peroxide at 240 nm ($\epsilon = 30 \text{ cm}^{-1}\text{M}^{-1}$) provided the value of the enzymatic activity (S4).

Synthesis of [(PNN)RuH(^xOH)(CO)] (2; 2-¹⁷O 2-¹⁸O). To a solution of complex 1 (81 mg, 0.18 mmol) in THF (5 ml) was added one equiv of H₂O (3.2 μl) and the mixture was stirred for one hr at room temperature. The ³¹P{¹H} NMR spectrum indicates 100% conversion to the hydroxo complex. The solvent was concentrated in volume and pentane (20 ml) was added to precipitate the product as a slightly yellow solid which was filtered and washed with pentane (3 × 0.5 ml). The reaction is reversed by heating or pumping on the solid. Therefore the exact isolated yield could not be determined and no elemental analysis could

be obtained. The procedure is the same for the reaction with H₂¹⁷O (**2-¹⁷O**) and H₂¹⁸O (**2-¹⁸O**). The spectroscopic data for **2-¹⁷O** and **2-¹⁸O** are virtually identical to these of **2** (unless mentioned otherwise).

Spectroscopic data for **2**: ³¹P{¹H} NMR (101.26 MHz, r. t.): δ = 108.30 (s, P^tBu₂, CD₂Cl₂), 109.91 (s, P^tBu₂, C₆D₆), 109.96 (s, P^tBu₂, toluene-d₈), 112.01 (s, P^tBu₂, THF-d₈) ppm. ¹H NMR (250.13 MHz, toluene-d₈, r. t.): δ = -14.88 (d, ²J_{PH} = 27.5 Hz, 1 H, Ru-H), -1.41 (br, 1 H, Ru-OH), 0.80 (t, ³J_{HH} = 7.0 Hz, 3 H, CH₂CH₃), 1.04 (t, ³J_{HH} = 7.0 Hz, 3 H, CH₂CH₃), 1.21 (d, ³J_{PH} = 13.0 Hz, 9 H, P(C(CH₃)₃)₂), 1.39 (d, ³J_{PH} = 13.5 Hz, 9 H, P(C(CH₃)₃)₂), 2.34 (m, 2 H, CH₂CH₃), 2.69 (dd, ²J_{HH} = 16.5 Hz, ²J_{PH} = 8.3 Hz, 1 H, PCH₂), 2.97 (dd, ²J_{HH} = 16.5 Hz, ²J_{PH} = 8.3 Hz, 1 H, PCH₂), 3.12 (dd, ²J_{HH} = 14.5 Hz, ⁴J_{PH} = 9.5 Hz, 1 H, py-NCH₂), 3.56 (m, 1 H, CH₂CH₃), 4.00 (m, 1 H, CH₂CH₃), 5.45 (d, ²J_{HH} = 14.5 Hz, 1 H, py-NCH₂), 6.37 (d, ³J_{HH} = 6.8 Hz, 1 H, py-H⁵), 6.54 (d, ³J_{HH} = 6.8 Hz, 1 H, py-H³), 6.87 (vt, ³J_{HH} = 7.0 Hz, 1 H, py-H⁴) ppm. ¹³C{¹H} NMR (125.76 MHz, THF-d₈, r. t.): δ = 8.50 (s, CH₂CH₃), 11.56 (s, CH₂CH₃), 29.88 (d, ²J_{PC} = 11.3 Hz, P(C(CH₃)₃)₂), 30.44 (s, P(C(CH₃)₃)₂), 35.51 (d, ¹J_{PC} = 25.2 Hz, P(C(CH₃)₃)₂), 37.56 (d, ¹J_{PC} = 23.0 Hz, P(C(CH₃)₃)₂), 37.85 (d, ¹J_{PC} = 11.5 Hz, PCH₂), 49.50 (s, CH₂CH₃), 54.70 (s, CH₂CH₃), 64.79 (s, py-NCH₂), 120.17 (s, py-C⁵), 120.73 (d, ³J_{PC} = 7.1 Hz, py-C³), 137.66 (s, py-C⁴), 161.92 (s, py-C⁶), 161.98 (s, py-C²), 209.22 (d, ²J_{PC} = 17.0 Hz, CO) ppm. IR (thin film, NaCl): $\tilde{\nu}$ = 2961m, 2085w (Ru-H), 1923vs (CO), 1600s, 1472s, 1072m, 1021m, 808m cm⁻¹. ESI-MS: *m/z* (%) = 453 (100) [M - OH]⁺.

Spectroscopic data for **2-¹⁷O**: ³¹P{¹H} NMR (202.47 MHz, THF-h₈, r. t.): δ = 112.14 (br, P^tBu₂) ppm. ¹H NMR (250.13 MHz, THF-h₈, r. t.): δ = -14.78 (d, ²J_{PH} = 27.6 Hz, 1 H, Ru-

H) ppm. $^{13}\text{C}\{\text{}^1\text{H}\}$ NMR (125.76 MHz, THF-*h*₈, r. t.): $\delta = 209.27$ (m, CO) ppm. ^{17}O NMR (68 MHz, THF-*h*₈, r. t.): $\delta = 32.43$ (s, 1 O, Ru–OH) ppm.

Synthesis of [(PNN-*D*₁)RuH(OD)(CO)] (2-*D*). To a solution of **1** (68 mg, 0.15 mmol) in THF (5 ml) was added one equiv of D₂O (3.0 μl) and the mixture was stirred for one hr at room temperature. The $^{31}\text{P}\{\text{}^1\text{H}\}$ NMR spectrum indicates 100% conversion to the hydroxo complex. The solvent was concentrated in volume and pentane (20 ml) was added to precipitate the product as a slightly yellow solid which was filtered and washed with pentane (3 \times 0.5 ml). The reaction is reversed by heating or pumping on the solid. Therefore the exact isolated yield could not be determined and no elemental analysis could be obtained.

$^{31}\text{P}\{\text{}^1\text{H}\}$ NMR (101.26 MHz, r. t.): $\delta = 108.05$ (s, *P*^{*t*}Bu₂, CD₂Cl₂), 110.18 (s, *P*^{*t*}Bu₂, THF-*d*₈) ppm. ^1H NMR (250.13 MHz, CD₂Cl₂, r. t.): $\delta = -15.52$ (d, $^2J_{\text{PH}} = 27.5$ Hz, 1 H, Ru–*H*), 0.84 (t, $^3J_{\text{HH}} = 7.1$ Hz, 3 H, CH₂CH₃), 1.03 (t, $^3J_{\text{HH}} = 7.0$ Hz, 3 H, CH₂CH₃), 1.24 (d, $^3J_{\text{PH}} = 13.0$ Hz, 9 H, P(C(CH₃)₃)₂), 1.41 (d, $^3J_{\text{PH}} = 13.5$ Hz, 9 H, P(C(CH₃)₃)₂), 2.78 (m, 2 H, CH₂CH₃), 2.83 (m, 1 H, PCHD), 3.48 (m, 1 H, CH₂CH₃), 3.75 (dd, $^2J_{\text{HH}} = 14.3$ Hz, $^4J_{\text{PH}} = 9.5$ Hz, 1 H, py-NCH₂), 3.87 (m, 1 H, CH₂CH₃), 5.23 (d, $^2J_{\text{HH}} = 14.3$ Hz, 1 H, py-NCH₂), 7.21 (d, $^3J_{\text{HH}} = 7.8$ Hz, 1 H, py-*H*⁵), 7.35 (d, $^3J_{\text{HH}} = 7.9$ Hz, 1 H, py-*H*³), 7.67 (vt, $^3J_{\text{HH}} = 7.8$ Hz, 1 H, py-*H*⁴) ppm. ^2D NMR (61.42 MHz, THF, r. t.): $\delta = -1.18$ (br, 1 D, Ru–OD), 2.83 (br, 1 D, PCHD) ppm. $^{13}\text{C}\{\text{}^1\text{H}\}$ NMR (125.76 MHz, C₆D₆, r. t.): $\delta = 8.16$ (s, CH₂CH₃), 11.21 (s, CH₂CH₃), 25.52 (d, $^1J_{\text{PC}} = 13.4$ Hz, PCHD), 29.33 (d, $^2J_{\text{PC}} = 8.4$ Hz, P(C(CH₃)₃)₂), 29.85 (s, P(C(CH₃)₃)₂), 34.74 (d, $^1J_{\text{PC}} = 27.0$ Hz, P(C(CH₃)₃)₂), 36.71 (d, $^1J_{\text{PC}} = 22.9$ Hz, P(C(CH₃)₃)₂), 49.08 (s, CH₂CH₃), 54.03 (s, CH₂CH₃), 67.53 (s, py-NCH₂), 119.38 (s, py-*C*⁵), 119.66 (d, $^3J_{\text{PC}} = 7.1$ Hz, py-*C*³), 136.51 (s, py-*C*⁴), 160.56 (s, py-*C*⁶),

161.10 (s, py-C²), 208.85 (d, ²J_{PC} = 16.8 Hz, CO) ppm. IR (thin film, NaCl): $\tilde{\nu}$ = 2959m, 2081w (Ru–H), 1922vs (CO), 1602s, 1473s, 1073m, 1019m, 807m cm⁻¹. ESI-MS: *m/z* (%) = 454 (100) [M – OD]⁺.

Synthesis of [(PNN)RuH(OH)(CO)-x(H₂O)] (2.nH₂O). (a) *Synthesis from 1 in benzene:*

To a dark red solution of **1** (91 mg, 0.20 mmol) in benzene (3 ml) was added a five fold excess of H₂O (20 μ l) and the mixture was stirred for 1 hr at room temperature. Then H₂O (1 ml) was added slowly to the reaction mixture at about 10 °C to form a lower layer. The product could be obtained as nearly colourless crystals at the phase boundary within three days. After filtration in the cold (10 °C) the product was washed with cold pentane (2 \times 0.5 ml). The reaction is reversed by heating or pumping on the solid. The crystals melt at room temperature due to the instability of the water layer. Therefore the yield could not be determined and elemental analysis could not be obtained. Due to the high intensity of the protons in the water layer, ¹H NMR spectrum is not available.

(b) *Synthesis from 1 in neat water:* To solid **1** (75 mg, 0.17 mmol) was added an excess of H₂O (1 ml) and the mixture was stirred for one day at room temperature. The ³¹P{¹H} NMR spectrum indicates 100% conversion to the hydroxo complex. The product thus obtained was not isolated.

³¹P{¹H} NMR (101.26 MHz, r. t.): δ = 104.73 (s, P^tBu₂, H₂O), 108.01 (s, P^tBu₂, CH₂Cl₂) ppm. ¹³C{¹H} NMR (125.78 MHz, H₂O, r. t.): δ = 9.91 (s, CH₂CH₃), 11.56 (s, CH₂CH₃), 29.71 (d, ²J_{PC} = 7.2 Hz, P(C(CH₃)₃)₂), 29.80 (d, ²J_{PC} = 5.7 Hz, P(C(CH₃)₃)₂), 36.41 (d, ¹J_{PC} = 26.4 Hz, P(C(CH₃)₃)₂), 37.10 (d, ¹J_{PC} = 15.1 Hz, P(C(CH₃)₃)₂), 51.29 (s, CH₂CH₃), 56.31 (s, CH₂CH₃), 66.14 (s, py-NCH₂), 121.19 (s, py-C⁵), 122.91 (d, ³J_{PC} = 15.1 Hz, py-C³), 140.29 (s, py-C⁴), 161.68 (s, py-C⁶), 163.30 (s, py-C²), 207.52 (d, ²J_{PC} = 14.6 Hz, CO) ppm.

UV/Vis (H₂O): λ_{abs} ($\epsilon/\text{cm}^{-1}\text{M}^{-1}$) = 345 (2319) nm. ESI-MS: m/z (%) = 453 (100) [M – OH]⁺.

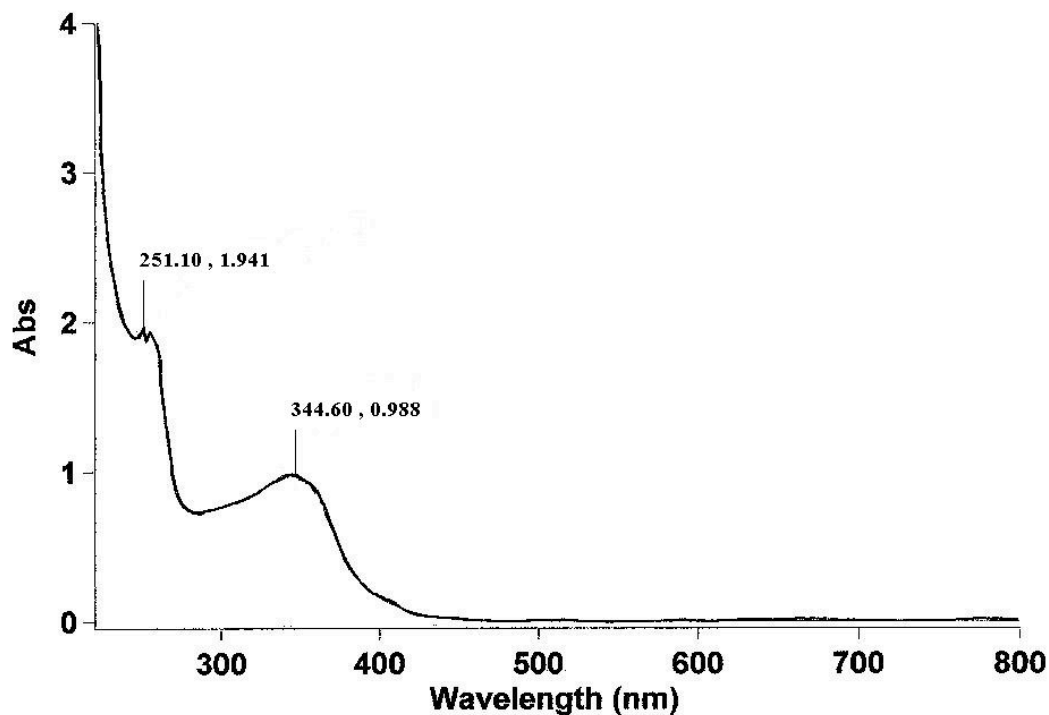


Fig S1. UV-Vis spectrum of complex 2. $C = 4.26 \times 10^{-4}$ mol/l in water

Synthesis of [(PNN-D₂)RuD(OD)(CO)-x(D₂O)] (2.nD₂O). The two different ways of synthesis are the same as described for the preparation of 2.nH₂O. D₂O was used instead of H₂O.

³¹P{¹H} NMR (101.26 MHz, D₂O, r. t.): $\delta = 104.71$ (s, P^tBu₂) ppm. ¹H NMR (250.13 MHz, D₂O, r. t.): $\delta = 1.02$ (m, 24 H, P(C(CH₃)₃)₂, CH₂CH₃), 2.83 (m, 4 H, CH₂CH₃), 2.89 (m, 2 H, CH₂CH₃), 3.05 (m, 2 H, CH₂CH₃), 3.98 (d, ²J_{HH} = 7.8 Hz, 1 H, py-NCH₂), 4.08 (d, ²J_{HH}

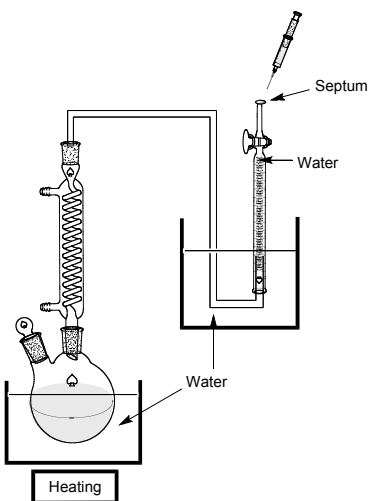
= 7.9 Hz, 1 H, py-NCH₂), 7.19 (d, ³J_{HH} = 7.8 Hz, 1 H, py-H⁵), 7.35 (d, ³J_{HH} = 7.7 Hz, 1 H, py-H³), 7.65 (vt, ³J_{HH} = 7.8 Hz, 1 H, py-H⁴) ppm. ²D NMR (61.42 MHz, H₂O, r. t.): δ = –18.61 (d, ²J_{PD} = 3.7 Hz, 1 D, Ru–D), –1.28 (br, 1 D, Ru–OD), 2.80 (br, 2 D, PCD₂) ppm. ¹³C{¹H} NMR (125.76 MHz, D₂O, r. t.): δ = 9.99 (s, CH₂CH₃), 11.57 (s, CH₂CH₃), 29.76 (d, ²J_{PC} = 7.2 Hz, P(C(CH₃)₃)₂), 29.79 (d, ²J_{PC} = 5.7 Hz, P(C(CH₃)₃)₂), 36.45 (d, ¹J_{PC} = 26.4 Hz, P(C(CH₃)₃)₂), 37.00 (d, ¹J_{PC} = 15.1 Hz, P(C(CH₃)₃)₂), 51.24 (s, CH₂CH₃), 56.28 (s, CH₂CH₃), 66.04 (s, py-NCH₂), 121.15 (s, py-C⁵), 122.90 (d, ³J_{PC} = 15.1 Hz, py-C³), 140.31 (s, py-C⁴), 161.66 (s, py-C⁶), 163.28 (s, py-C²), 207.50 (d, ²J_{PC} = 14.6 Hz, CO) ppm. ESI-MS: *m/z* (%) = 456 (100) [M – OD]⁺.

Synthesis of [(PNN)Ru(^xOH)(^yOH)(CO)] (3: x = y = 16; 3-¹⁶O¹⁸O: x = 16, y = 18;

3-¹⁸O¹⁸O: x = y = 18). (a) *Synthesis of 3 from 2 by heating in water, and determination of evolved H₂*: **2** (83 mg) was dissolved in H₂O (5 ml) in a flask equipped with a reflux condenser. The condenser was connected via a thin, s-shaped (sigmoidal) glass tube to a pneumatic device incorporating a small burette (10 ml) (see schematic drawing below) and the whole system was flushed with argon. The solution was refluxed for three days, during which time the colour of the solution changed from colourless to greenish and hydrogen was evolved. The volume of the H₂ which was collected in the small burette was 1.55 ml (39%). Quantification of H₂ in the gas phase of the reaction vessel by GC gives a yield of 37%. H₂ was detected also by reaction of a sample of the gas phase with Ir(PEt₃)₃Cl (S3) to form *mer-cis*-(PEt₃)₃Ir(H)₂Cl (S5) (Scheme 1 below).

After evaporating the solvent, the residue was dissolved in THF (1.5 ml) and diethyl ether (15 ml) was added to precipitate the product together with some unidentified by-

products. Recrystallization from benzene/water gave the desired complex as a green solid in a yield of 45%.



For the synthesis of complex **3** (without determination of the evolved hydrogen) the same procedure was performed under Argon in an open system not connected to the pneumatic device.

Schematic drawing of the system used in the experiment (a) above

(b) *Independent synthesis of 3 from 2 with N₂O*: Into a solution of **2** (~79 mg, after drying the crystals in a stream of nitrogen at 10 °C) in THF (5 ml) was bubbled N₂O for 10 min. at room temperature. The reaction mixture was stirred overnight during which time its colour changed from colourless to green. The solvent was concentrated in volume and diethyl ether (20 ml) was added to precipitate the product. After filtering, the residue was washed with diethyl ether (3 × 0.5 ml) to yield the product as a dark green microcrystalline powder (49 mg, 60% relative to **2** without the water layer).

Synthesis of **3**-¹⁶O¹⁸O: complex **2**-¹⁸O was treated with N₂O (analogous to procedure (b) for **3**). Synthesis of **3**-¹⁸O¹⁸O: complex **2**-¹⁸O was treated with H₂¹⁸O (analogous to procedure (a) for **3**). If not mentioned otherwise, the spectroscopic data for **3**-¹⁶O¹⁸O and **3**-¹⁸O¹⁸O are virtually identical to these of **3**.

Spectroscopic data for **3**: $^{31}\text{P}\{^1\text{H}\}$ NMR (101.26 MHz, CD_2Cl_2 , r. t.): $\delta = 93.96$ (s, P^tBu_2) ppm. ^1H NMR (250.13 MHz, CD_2Cl_2 , r. t.): $\delta = -7.4$ (br, 2 H, OH), 1.16 (d, $^3J_{\text{PH}} = 13.0$ Hz, 9 H, $\text{P}(\text{C}(\text{CH}_3)_3)_2$), 1.17 (t, $^3J_{\text{HH}} = 7.0$ Hz, 3 H, CH_2CH_3), 1.21 (t, $^3J_{\text{HH}} = 7.0$ Hz, 3 H, CH_2CH_3), 1.48 (d, $^3J_{\text{PH}} = 14.3$ Hz, 9 H, $\text{P}(\text{C}(\text{CH}_3)_3)_2$), 2.69 (m, 1 H, CH_2CH_3), 2.85 (m, 1 H, CH_2CH_3), 3.14 (m, 1 H, CH_2CH_3), 3.25 (m, 1 H, CH_2CH_3), 3.29 (dd, $^2J_{\text{HH}} = 17.0$ Hz, $^2J_{\text{PH}} = 7.5$ Hz, 1 H, PCH_2), 3.64 (dd, $^2J_{\text{HH}} = 17.0$ Hz, $^2J_{\text{PH}} = 8.0$ Hz, 1 H, PCH_2), 3.99 (dd, $^2J_{\text{HH}} = 14.8$ Hz, $^4J_{\text{PH}} = 3.0$ Hz, 1 H, py-N CH_2), 4.53 (d, $^2J_{\text{HH}} = 14.8$ Hz, 1 H, py-N CH_2), 7.24 (d, $^3J_{\text{HH}} = 7.8$ Hz, 1 H, py- H^5), 7.39 (d, $^3J_{\text{HH}} = 7.8$ Hz, 1 H, py- H^3), 7.68 (vt, $^3J_{\text{HH}} = 7.8$ Hz, 1 H, py- H^4) ppm. $^{13}\text{C}\{^1\text{H}\}$ NMR (125.76 MHz, CD_2Cl_2 , r. t.): $\delta = 8.46$ (s, CH_2CH_3), 9.47 (s, CH_2CH_3), 29.09 (s, $\text{P}(\text{C}(\text{CH}_3)_3)_2$), 30.75 (d, $^2J_{\text{PC}} = 3.8$ Hz, $\text{P}(\text{C}(\text{CH}_3)_3)_2$), 37.06 (d, $^1J_{\text{PC}} = 16.1$ Hz, $\text{P}(\text{C}(\text{CH}_3)_3)_2$), 38.08 (d, $^1J_{\text{PC}} = 12.6$ Hz, $\text{P}(\text{C}(\text{CH}_3)_3)_2$), 38.37 (d, $^1J_{\text{PC}} = 23.0$ Hz, PCH_2), 44.72 (s, CH_2CH_3), 51.55 (s, CH_2CH_3), 62.88 (s, py-N CH_2), 120.45 (s, py- C^5), 121.66 (d, $^3J_{\text{PC}} = 8.0$ Hz, py- C^3), 137.76 (s, py- C^4), 161.29 (s, py- C^6), 164.30 (s, py- C^2), 207.44 (d, $^2J_{\text{PC}} = 16.1$ Hz, CO) ppm. IR (thin film, NaCl): $\tilde{\nu} = 3413\text{br}$ (^{16}OH), 3399br (^{18}OH , **5b**, **5c**), 2953m, 1923vs (CO), 1594s cm^{-1} . UV/Vis (H_2O): λ_{abs} ($\epsilon/\text{cm}^{-1}\text{M}^{-1}$) = 380 (8157), 459 (2045), 716 (505) nm. ESI-MS: m/z (%) = 469 (18) $[\text{M} - \text{OH}]^+$, 453 (100) $[\text{M} - \text{OOH}]^+$ (this fragment might result from H_2O_2 elimination + protonation). Anal. Calc. for $\text{C}_{20}\text{H}_{37}\text{N}_2\text{O}_3\text{PRu}$: C, 49.47; H, 7.68; N, 5.77. Found: C, 49.33; H, 7.62; N, 5.73.

Calculations at the PCM(H_2O)-M06/SDB-cc-pVDZ//M06/SDD(d) level of theory on the $\text{PMe}_2/\text{NMe}_2$ model of **3** show that the (unknown) *trans*-(PNN)Ru(CO)(OH) $_2$ is less stable than the *cis* isomer (by $\Delta G(298) = 1.7$ kcal/mol).

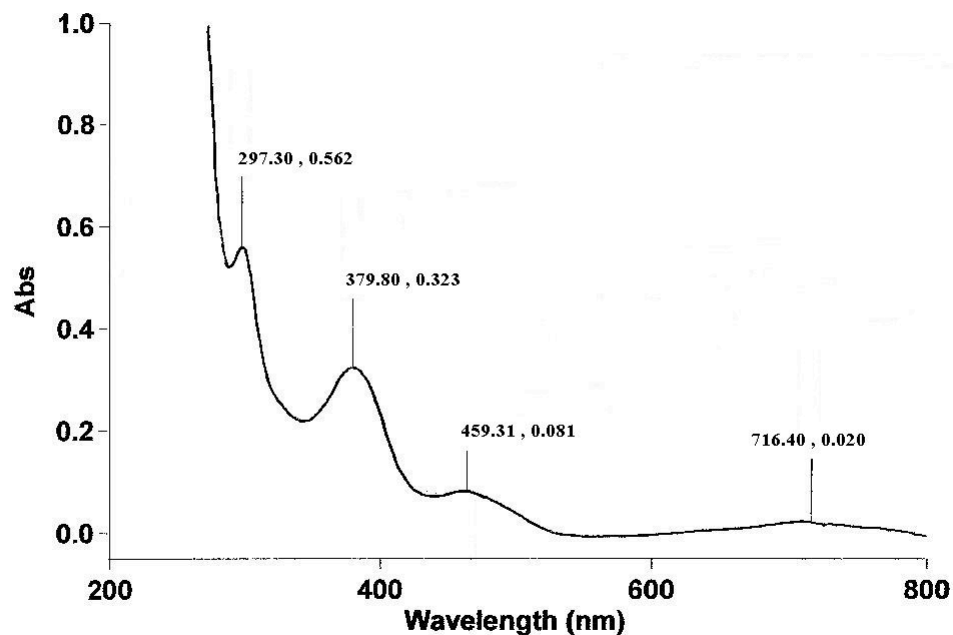
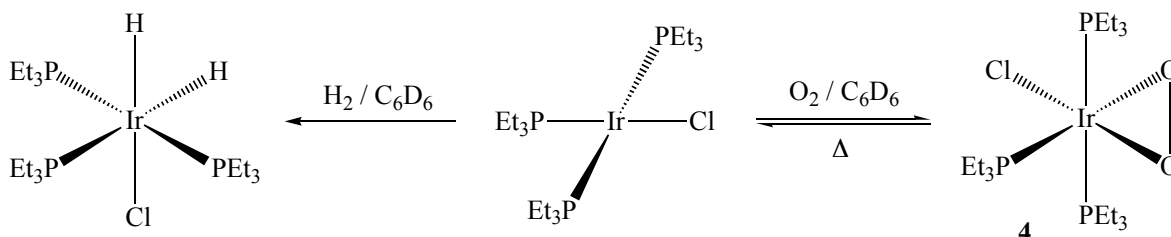


Fig. S2. UV-Vis spectrum of complex **3**. $C = 3.96 \times 10^{-5}$ mol/l in water

Synthesis of [(PEt₃)₃Ir(O₂)Cl] (4**).** To a solution of (PEt₃)₃IrCl (0.09 mmol, *S3*) in benzene (3 ml) was injected one equiv of dioxygen (2 ml) and stirred at room temperature for 5 min during which time its colour changed from orange to slightly yellow. The solvent was concentrated in volume and pentane (15 ml) was added to precipitate the product. After filtering, the residue was washed with pentane (3 × 0.5 ml) to yield the product as a slightly yellow microcrystalline powder (52 mg, 94%).

Spectroscopic data for **4**: ³¹P{¹H} NMR (161.98 MHz, C₆D₆, r. t.): δ = -13.64 (vt, ²J_{PP} = 15.6 Hz, 1 P, Ir-P_AEt₃), -14.37 (d, ²J_{PP} = 15.6 Hz, 2 P, Et₃P_B-Ir-P_BEt₃) ppm. ¹H NMR (400.13 MHz, C₆D₆, r. t.): δ = 0.95 (m, 9 H, P_ACH₂CH₃), 1.10 (m, 18 H, P_BCH₂CH₃), 1.70 (m, 6 H, P_BCH₂CH₃), 1.85 (m, 6 H, P_ACH₂CH₃), 2.07 (m, 6 H, P_BCH₂CH₃) ppm. ¹³C{¹H} NMR (125.76 MHz, C₆D₆, r. t.): δ = 8.54 (s, P_BCH₃), 8.73 (s, P_ACH₂), 13.52 (vt, ¹J_{PC} =

$^3J_{\text{PCtrans}} = 15.3 \text{ Hz}$, P_{BCH_2} , 21.42 (d, $^1J_{\text{PC}} = 30.5 \text{ Hz}$, P_{ACH_2}) ppm. IR (thin film, NaCl): $\tilde{\nu} = 2962\text{s}$, 2939s, 2884s, 1464m, 1425m, 1378w, 1261w, 1035vs, 840m (O–O), 762m cm^{-1} . ESI-MS: m/z (%) = 615 (32) $[\text{M} + \text{H}]^+$, 547 (100) $[\text{M} - \text{O}_2 - \text{Cl}]^+$.



Scheme S1

Procedure for irradiation and dioxygen quantification.

(a) The *cis* dihydroxo complex **3** (61.3 mg, 0.13 mmol) was dissolved in water or THF (17 ml) in a thin-walled glass (pyrex) reaction vessel with an accurate volume of 20 ml (3 ml gas phase). The vessel was sealed with a rubber septum and Teflon stripes and irradiated with a 300 W halogen lamp for two days using a 1 cm Perspex filter. An exact volume between 0.5 and 2 ml of the gas phase was withdrawn from the reaction in water with a syringe and introduced into a solution containing excess of $(\text{PEt}_3)_3\text{IrCl}$ (**S3**) in benzene- d_6 (NMR tube, 1.2 ml). The quantification was done by integrating and comparing the peaks of the starting material and the newly formed, side-on dioxygen complex $(\text{PEt}_3)_3\text{Ir}(\text{O}_2)\text{Cl}$ (**4**) in the $^{31}\text{P}\{^1\text{H}\}$ NMR spectrum.

This procedure was repeated three times with different gas volumes and the average yield of the released dioxygen was calculated to be 23% (34% based on reacted **3**). The compounds which were produced during the irradiation were not isolated. The characterisation was done by the comparison of the NMR spectra with the known compounds. The following complexes were found in both solvents: the hydrido-hydroxo

complex **2.nH₂O** (45%), unreacted **3** (33%) and unidentified products (22%, most probably phosphine oxides). When irradiation of **3** was performed in water under argon flow to remove the generated O₂, clean conversion of **3** (49%) to **2.nH₂O** (49%) was observed, with no by-products being formed.

(b) Irradiation of the *cis* dihydroxo complex **3** (22 mg, 0.045 mmol) in 1.9 ml of water, in a sealed NMR screw-cap tube with an accurate volume of 4.6 ml (2.7 ml argon gas phase), with a 300 W halogen lamp using a Perspex filter for 12 hours resulted in a colour change of the solution from green to greenish-yellow and dioxygen was evolved. ³¹P{¹H} NMR spectra of the aqueous reaction mixture exhibits hydrido-hydroxo complex **2** (45%) formed upon irradiation and the residual dihydroxo complex **3** (55%). At this stage formation of by-products was not observed. An exact volume of 50 µl was withdrawn with a syringe from the NMR tube gas phase and injected into GC/MS, calibrated earlier with three known O₂/Ar gas mixtures in the same type of NMR tubes, over the same volume of water. The gas, liberated upon irradiation, was identified by GC/MS as dioxygen obtained in 24% yield. In addition, a volume of 1 ml was withdrawn with a syringe from the NMR tube gas phase and introduced into a C₆D₆ solution of the complex (PEt₃)₃IrCl. ³¹P{¹H} NMR of the C₆D₆ solution revealed formation of the side-on dioxygen complex (PEt₃)₃Ir(O₂)Cl and the presence of residual (PEt₃)₃IrCl complex. Integration ratio between the two complexes reveals that the dioxygen yield is 23%.

After irradiation of the reaction mixture for additional 12 hrs the reaction mixture contained: unreacted di-hydroxo complex **3** (47%), the hydrido-hydroxo complex **2** (29%) and some non identified by-products (24%) (by ³¹P{¹H} NMR).

[c] Irradiation of di-hydroxo complex **3** (12 mg) in water (1.0 ml), in an NMR screw-cap tube under argon bubbling, with a 300 W halogen lamp using a Perspex filter for 24 hrs resulted in a colour change of the solution from green to greenish-yellow. $^{31}\text{P}\{^1\text{H}\}$ NMR of the reaction mixture revealed unreacted dihydroxo complex **3** (51%) and the hydrido-hydroxo complex **2** (49%). Under argon bubbling formation of by-products was not observed even after 24 hours of irradiation (rather than in a sealed system).

[d] Notes regarding GC/MS measurements of the isotopic distributions:

It is very important to “wash” the syringe at least 3 times with the atmosphere in the reaction vessel. Procedure:

- penetrate the rubber/Teflon septum; because of the over pressure the syringe will be filled automatically.
- repeat this three to five times
- fill the syringe with more gas than it is necessary for the GC-MS experiment
- before injecting the gas into the GC-MS, release the excess of gas near the septum of the GC and then immediately introduce the gas to GC

Estimation of quantum yield

The photochemical quantum yield was estimated by the determination of the amount of complex **2** formed (Scheme 2) relative to the number of photons supplied. The power density of the illuminating beam at the spectral range 320-450 nm was measured by placing an Ophir thermal head power-meter at the place of the reaction vessel. A Perspex filter and a short pass 450 nm filter were placed between the source and the thermal head. The conversion of the power density to a photon flux was done assuming the average energy of

the photons to be ~ 3.1 eV (~ 400 nm). The measured power density was 3.5 mW/cm² corresponding to a flux of $\sim 7 \times 10^{15}$ photons/cm²sec. Based on an estimated optical density of the reactant during the progress of the reaction in experiment (b) above, the reaction time, and the irradiated area, the quantum yield is approximately 5%.

Procedure for the decomposition of H₂O₂ by complex 1. To an aqueous solution of hydrogen peroxide (0.1 mol/l, 1.0 ml) in THF (1.5 ml) a solution of **1** in THF ($c = 5 \times 10^{-6}$ mol/l, 100 μ l) was added at room temperature under stirring. Gas evolution was observed immediately. Part of the gas phase was withdrawn with a syringe and identified as dioxygen with GC/MS and chemically by the reaction with (PEt₃)₃IrCl to form the side-on dioxygen Ir(III) complex **4**. In addition, the NMR spectrum exhibits characteristic resonances for the iridium(III) hydrido-hydroxo complex *mer-cis*-(PEt₃)₃Ir(H)(OH)Cl formed by oxidative addition of water (*S5*).

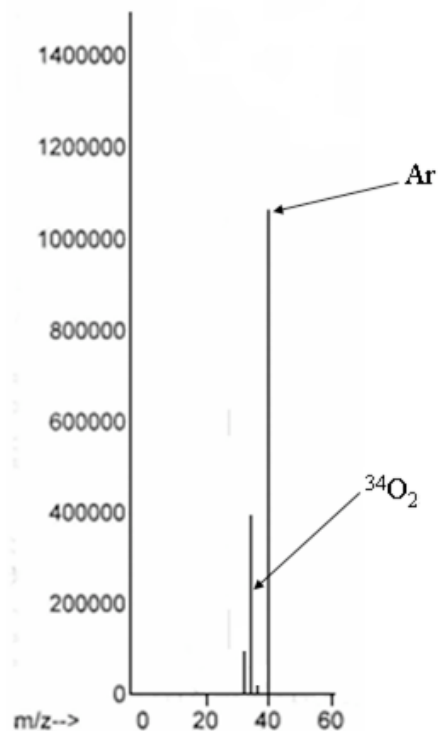
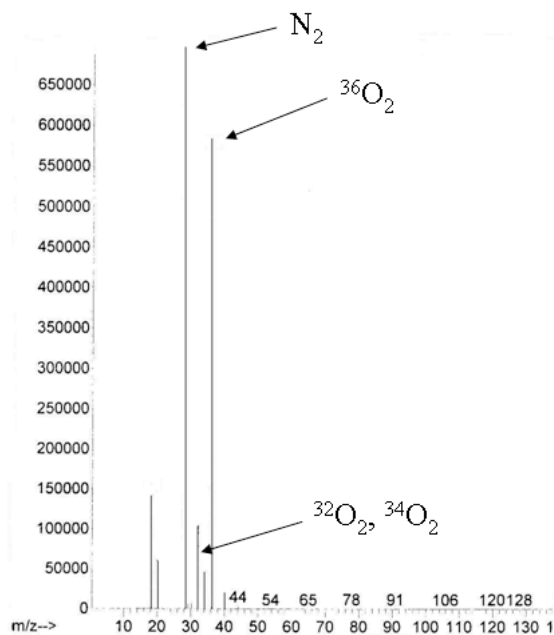


Fig. S3. Mass spectrum of a gaseous extract from the photolytic reaction of isotopically labelled dihydroxo complexes (a) *left*: $3\text{-}^{18}\text{O}^{18}\text{O}$ (reaction under N_2). Ratios obtained: $^{32}\text{O}_2\text{:}^{34}\text{O}_2\text{:}^{36}\text{O}_2$ 2.3:1:12.9 (b) *right*: $3\text{-}^{16}\text{O}^{18}\text{O}$ (reaction under Ar). Ratios obtained: $^{32}\text{O}_2\text{:}^{34}\text{O}_2\text{:}^{36}\text{O}_2$ 3.8:16.2:1

Cross-over experiment: irradiation of $3\text{-}^{18}\text{O}^{18}\text{O}$ + $3\text{-}^{16}\text{O}^{16}\text{O}$

The *cis* dihydroxo complex $3\text{-}^{18}\text{O}^{18}\text{O}$ (34.0 mg, 0.07 mmol) and the *cis* dihydroxo complex $3\text{-}^{16}\text{O}^{16}\text{O}$ (34.2 mg, 0.07 mmol) were dissolved in water (4 ml) in a thin-walled glass reaction vessel and irradiated with a 300 W halogen lamp in an argon atmosphere for two days using a 1 cm Perspex filter. During this time two different isotopes of dioxygen ($^{32}\text{O}_2$, $^{36}\text{O}_2$) were evolved and detected with GC/MS (see Fig. 2 in manuscript) and by introducing 1 ml of the gas phase into a solution of $(\text{PEt}_3)_3\text{IrCl}$ (0.02 mmol, S3) in benzene- d_6 (NMR

tube, 1.0 ml). The following ratio between the dioxygen isotopes was obtained: $^{32}\text{O}_2$: $^{34}\text{O}_2$: $^{36}\text{O}_2$ 13.1:1:15.6 (corrected for ^{36}Ar isotope (abundance 0.337%) contribution)

Experimental for the irradiation of $3\text{-}^{16}\text{O}^{18}\text{O}$:

The *cis* dihydroxo complex $3\text{-}^{16}\text{O}^{18}\text{O}$ (44.0 mg, 0.09 mmol) was dissolved in water (4 ml) in a thin-walled glass reaction vessel and irradiated in an argon atmosphere with a 300 W halogen lamp for two days using a 1 cm Perspex filter. During this time mainly one isotope of dioxygen ($^{34}\text{O}_2$) was evolved and detected with GC/MS. The following ratio between the dioxygen isotopes was obtained: $^{32}\text{O}_2$: $^{34}\text{O}_2$: $^{36}\text{O}_2$ 3.8:16.2:1

Experimental details of Single Crystal X-ray Diffraction of $2.n\text{H}_2\text{O}$

A yellow plate-like crystal of $2.n\text{H}_2\text{O}$ having approximate size of $0.35 \times 0.20 \times 0.10 \text{ mm}^3$ was placed in Hampton Paraton-N oil, mounted in a MiTeGen loop and flash frozen to 120(2) K with an Oxford Cryosystem Coldstream. Measurements were made on a Nonius KappaCCD diffractometer with graphite monochromatic MoK_α radiation ($\lambda = 0.7107$) to a maximum 2θ value of 55.00° with a detector to crystal distance of 36.0 mm and a frame width of 1.0° for a total of 60 seconds per frame. The data frames were processed and scaled with the HKL Denzo software package. Compound $2.n\text{H}_2\text{O}$ crystallized in space group C2/c (no. 15) with unit cell parameters $a=39.3120(9) \text{ \AA}$, $b=10.7693(3) \text{ \AA}$, $c=16.1683(3) \text{ \AA}$, $\beta=96.5731(13)^\circ$. The structure was solved with SHELXS by direct methods and refined with full matrix least squares refinement based on F^2 in SHELXL-97. There is one $2.n\text{H}_2\text{O}$ molecule per asymmetric unit, 8 per unit cell however, in addition to

the molecular packing, the crystal contains two ordered solvent layers, encompassing a total of 42.5% of the cell volume. One solvent layer is comprised of benzene and the other of two alternate arrangements of water molecules. The oxygen atoms of the water layers were located from the $|F_o-F_c|$ and $|2F_o-F_c|$ electron density maps using the program COOT (S6). The two alternate arrangements of oxygen atoms were determined on the basis of hydrogen bonding distances and mutually exclusive positions, although due to the nature of this layer, hydrogen atoms on these solvent oxygen atoms were not located. The O2 hydroxyl of the Ru atom is hydrogen bonded to oxygen O3 that is found in both water layer arrangements, which in turn makes hydrogen bonds to the network of oxygen atoms in the water layers (see Tables S2 and S3 and Figures S4-S6).

Table S1. Crystal data and structure refinement for **2.nH₂O**

Empirical formula	C ₂₆ H ₄₄ N ₂ O _{8.62} PRu	
Formula weight	654.67	
Temperature	120(2) K	
Wavelength	0.71073 Å	
Crystal system	Monoclinic	
Space group	C2/c (no. 15)	
Unit cell dimensions	a = 39.3120(9) Å	α = 90°
	b = 10.7693(3) Å	β = 96.5730(13)°
	c = 16.1683(3) Å	γ = 90°
Volume	6800.1 Å ³	
Z	8	
Density (calculated)	1.279 Mg/m ³	
Absorption coefficient	0.552 mm ⁻¹	
F(000)	2736	
Crystal size	0.35 × 0.20 × 0.10 mm ³	
Theta range for data collection	2.68 to 27.48°	
Index ranges	0 ≤ h ≤ 50, 0 ≤ k ≤ 13, -20 ≤ l ≤ 20	
Reflections collected	29007	
Independent reflections	8147 [R(int) = 0.0480]	
Completeness to theta = 27.48°	99.2%	
Absorption correction	None	
Max. and min. transmission	0.9468 and 0.8301	
Refinement method	Full-matrix least-squares on F ²	
Data / restraints / parameters	7721 / 0 / 420	
Goodness-of-fit on F ²	1.012	
Final R indices [I > 2σ(I)]	R1 = 0.0403, wR2 = 0.0904	
R indices (all data)	R1 = 0.0587, wR2 = 0.0988	
<u>Largest diff. peak and hole</u>	<u>1.426 and -0.789 eÅ⁻³</u>	

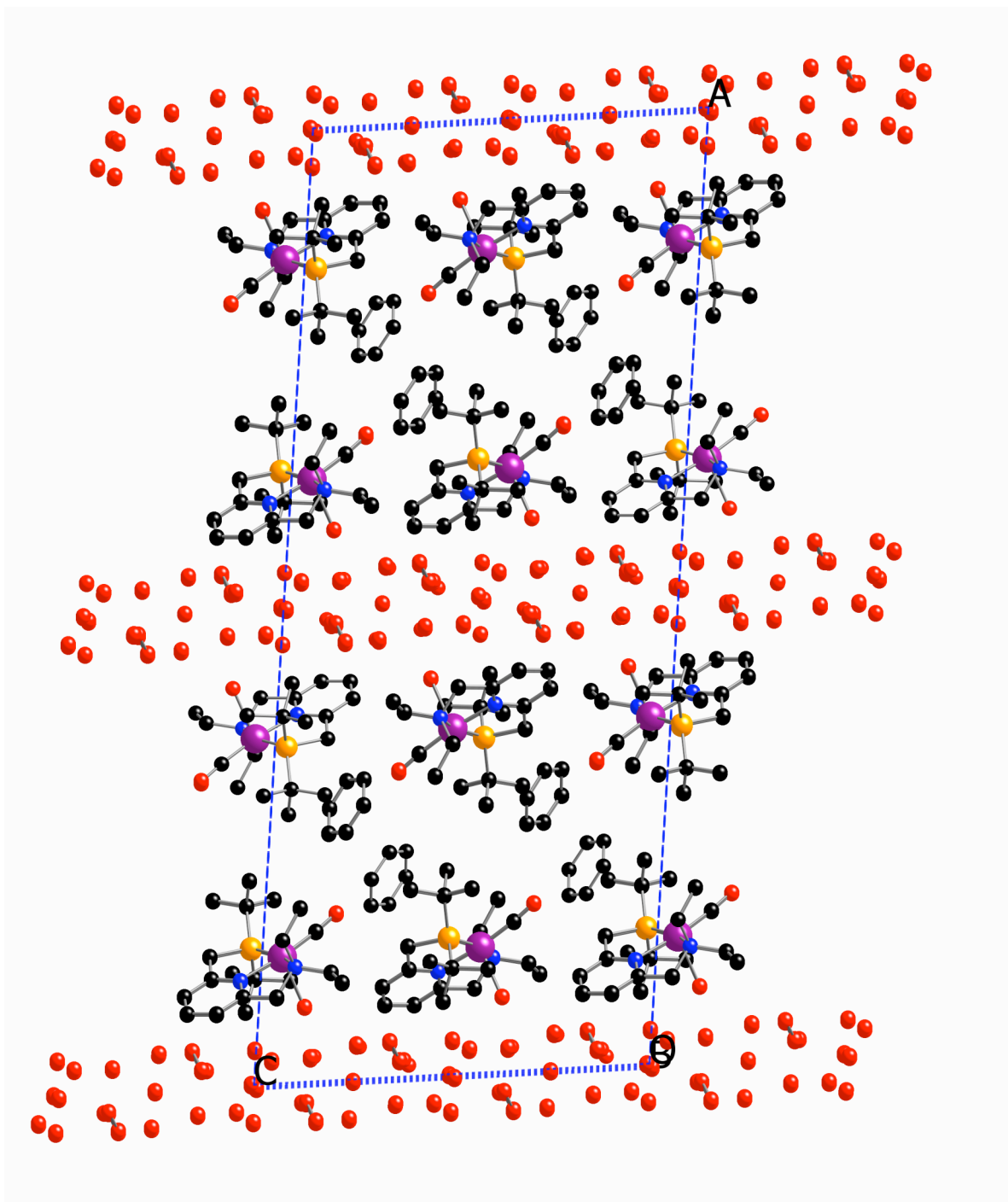


Fig. S4. Packing diagram viewed down y-axis showing the arrangement of the layered water and benzene molecules and the Ru complexes in $2.nH_2O$. Hydrogen atoms are omitted. Oxygen (red), nitrogen (blue), ruthenium (purple), phosphorus (yellow).

Table S2. Interatomic distances (Å) for H-bonding interactions of water molecules in subunit (layer) 1.

6-member ring (O3, O4, O7, O10a, O13, O8a)

O3...O4	2.851
O4...O7	2.772
O7...O10a	2.556
O10a...O13	2.776
O13...O8a	2.574
O8a...O3	2.631

5-member ring (O2, O3, O8a, O9a, O9a')

O2...O3	2.616
O3...O8a	2.852
O8a...O9a	2.824
O9a...O9a'	2.989
O9a'...O2	2.740

6-member ring (O2, O3, O4, O11, O4', O9a)

O2...O3	2.616
O3...O4	2.851
O4...O11	2.736
O11...O4'	2.736
O4'...O9a	2.775
O9a...O2	2.740

5-member ring (O4, O3, O2, O9a, O9a')

O4...O3	2.851
O3...O2	2.616
O2...O9a	2.740
O9a...O9a'	2.989
O9a'...O4	2.775

6-member ring (O2, O3, O8a', O13, O8a, O9a)

O2...O3	2.616
O3...O8a'	2.631
O8a...O13	2.574
O13...O8a'	2.574
O8a'...O9a	2.824
O9a...O2	2.740

5-member ring (O11, O4, O9a, O9a', O4')

O11...O4	2.736
O4...O9a	2.775
O9a...O9a'	2.989
O9a'...O4	2.775
O4'...O11	2.736

4-member ring (O3, O8a, O3', O8a')

4-member ring (O10a, O11, O10a', O13)

O10a...O11	2.742
O11...O10a'	2.742
O10a'...O13	2.776

O3...O8a 2.631

O3...O8a' 2.852

4-member ring (O4, O3, O8a', O9a)

O4...O3 2.851

O3...O8a' 2.852

O8a'...O9a 2.824

O9a'...O4 2.775

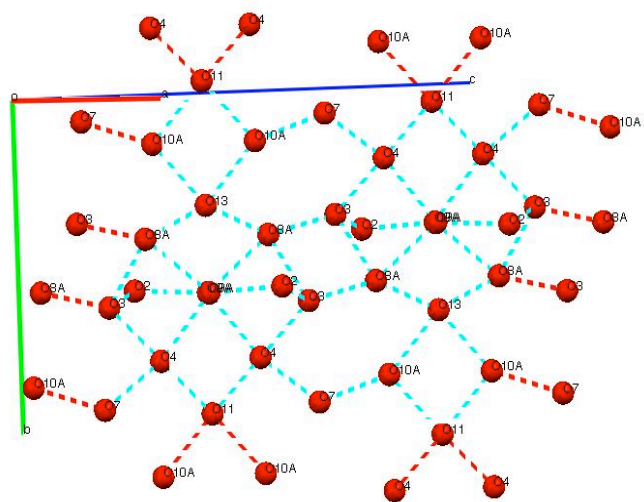
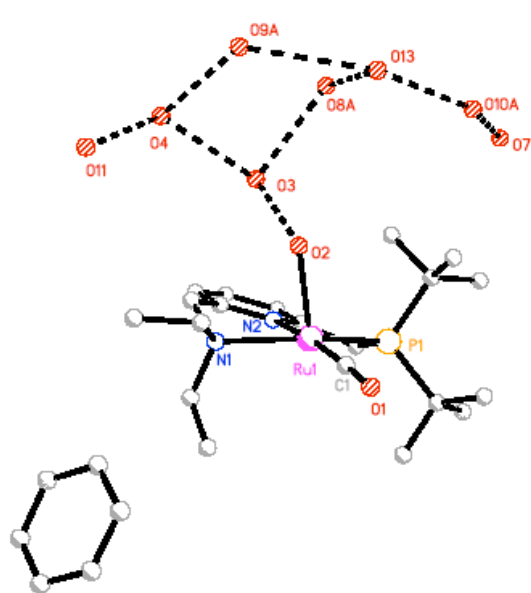


Fig. S5. Network of water layer of complex $2.nH_2O$ (layer/subunit 1)

Table S3. Interatomic distances (Å) for H-bonding interactions of water molecules in subunit (layer) 2.

<u>7-member ring (O2, O3, O6, O5, O12, O5', O9b)</u>		<u>5-member ring (O3, O8b, O13, O10b, O6)</u>	
O2...O3	2.616	O3...O8	2.948
O3...O6	2.769	O8b...O13	2.775
O6...O5	2.793	O13...O10b	2.357
O5...O12	2.758	O10b...O6	2.735
O12...O5'	2.758	O6...O3	2.769
O5'...O9b	2.816		
O9b...O2	2.746		
<u>6-member ring (O2, O3, O8b, O13, O8b', O9b)</u>		<u>4-member ring (O3, O8b, O3', O8b')</u>	
O2...O3	2.616	O3...O8b	2.649
O3...O8b	2.649	O8b...O3'	2.948
O8b...O13	2.775	O3'...O8b'	2.649
O13...O8b'	2.775	O3b'...O3	2.948
O8b'...O9b	2.793		
O9b...O2	2.746		
<u>5-member ring (O3, O6, O5, O9b, O8b)</u>		<u>4-member ring (O10b, O12, O10b', O13)</u>	
O3...O6	2.769	O10b...O12	2.734
O6...O5	2.793	O12...O10b'	2.734
O5...O9b	2.816	O10b'...O13	2.357
O9b...O8b	2.793	O13...O10b	2.357
O8b...O3	2.649		

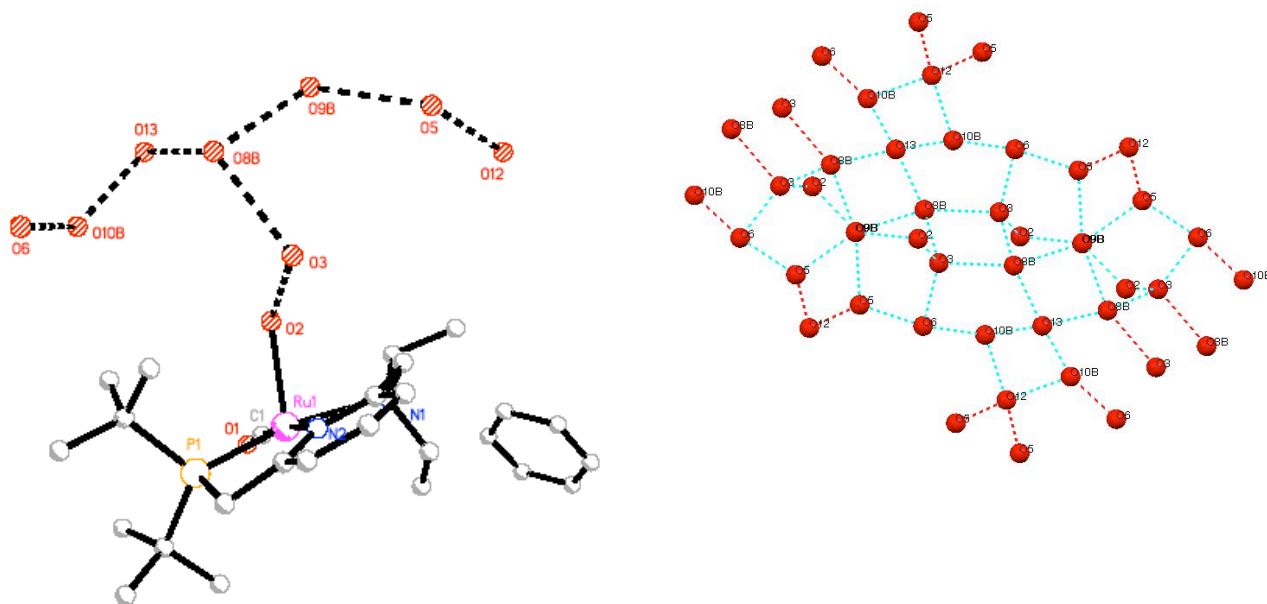


Fig. S6. Network of water layer of complex $2.nH_2O$ (layer/subunit 2)

Experiments for Detection of OH Radicals

Irradiation of the dihydroxo complex 3 in the presence of DMPO

To a solution of the dihydroxo complex **3** (200 μ l, 5×10^{-3} mol/l) in H_2O was added DMPO (200 μ l, 0.18 mol/l) and then the mixture was irradiated (300 W halogen lamp, 1cm Perspex filter) in a screw cap NMR tube for 16 hrs under an atmosphere of nitrogen. 100 μ l of the reaction mixture were transferred to an EPR flat cell and the spectrum was recorded. Experimental conditions: microwave power 20 mW, modulation amplitude 1 G, temperature 293 K.

Performing the irradiation of **3** in the presence of the spin trap 5,5-dimethyl-1-pyrroline-1-oxide (DMPO) (32), we observed that OH radicals are formed, as evidenced by the EPR spectrum (Fig. 3a) which shows the typical quartet for the DMPO-OH radical spin adduct (1 : 2 : 2 : 1, $a_N = a_H = 14.9$ G, (32, S7). In order to exclude the possibility that the DMPO-OH spin adduct was produced by the decomposition of DMPO-OOH (S8), DMSO (~5-10%) was added to an aqueous solution of **3** before irradiation. DMSO reacts with the liberated hydroxyl radicals to form carbon centred $\cdot\text{CH}_3$ -radicals. These methyl radicals react with DMPO to give the DMPO-CH₃ spin adduct producing the characteristic sextet EPR spectrum (S9). Indeed, we observed the sextet spectrum ($a_N = 15.5$ G, $a_H = 22.6$ G) with different intensities correlating with the concentration of DMSO (Fig. 3b). Other routes that can, in principle, lead to this spin adduct were excluded (see below). In principle, the quartet could also be obtained by the reaction of singlet oxygen (formed by energy transfer from Ru(II)* excited state) with DMPO (S10). Life-time of the singlet oxygen in D₂O is much longer than in H₂O, therefore the EPR signal of the spin adduct in that case should be five to ten times more intensive (S11). However, no difference in the intensity of the EPR signal was found when irradiation experiments were performed in D₂O, therefore we believe that singlet oxygen is not involved in the reaction with the spin trap. To recheck this statement, we irradiated **3** in the presence of tetramethylpiperidine (TEMP), which forms with singlet oxygen a characteristic triplet EPR spectrum, $a_N = 15.7$ G (S12) of the tetramethylpiperidine-N-oxide (TEMPO). No EPR signal was observed in this case.

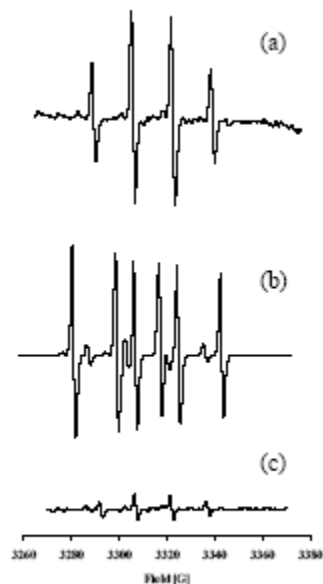
Our experiments clearly indicate that the hydroxyl radicals are not the source of the liberated O₂. If OH-radicals play an important role in the formation of hydrogen peroxide

or dioxygen, no gas evolution should be observed by adding an OH radical scavenger such as *tert*-butanol to the reaction mixture (30). We found that in the presence of this alcohol, the amount of produced dioxygen was virtually the same as without. Presumably, the hydroxyl radicals were formed by a Fenton type reaction (32) catalyzed by Ru(II) or by light induced decomposition of H₂O₂, released from **3** by reductive elimination (Scheme 4). It is worthwhile to mention that *no* OH-radicals were detected with EPR techniques when we irradiated the hydrido-hydroxo complex **2.nH₂O**.

Supporting evidence that hydrogen peroxide is the source of hydroxyl radicals in the light reaction were obtained based on experiments with the enzyme Catalase. It is expected that if H₂O₂ is the source of hydroxyl radicals, its interception by Catalase will prevent their formation. Indeed, the intensity of the observed EPR signal of the DMPO-OH spin adduct significantly decreases in the presence of Catalase (Fig S5c) (S7). The amount of evolved O₂ was slightly larger (by 1-2%) than in the absence of added Catalase .

Fig. S7. X-band EPR spectra of the (a) DMPO- \cdot OH spin adduct formed by the irradiation of the dihydroxo complex **3** (b) the DMPO- \cdot CH₃ spin adduct formed by the irradiation of **3** in the presence of 7% of DMSO (c) X-band EPR spectrum of the DMPO- \cdot OH spin adduct in the presence of Catalase ($\sim 10^{-10}$ M).

Experimental conditions: microwave power 20 mW, modulation amplitude 1 G, temperature 293 K, in water.



Experimental details for the activity check of the enzyme Catalase and for EPR-based experiments.

(a) *Activity check of Catalase:* Enzymatic activity of Catalase was assessed by adding the solution of enzyme in water containing a sodium phosphate buffer 10mM, pH 7.5 (3×10^{-9} mol/l, 100 μ l) to a solution of hydrogen peroxide (2.2×10^{-2} mol/l, 4.5 ml) in water at room temperature using quartz cuvettes (1 cm). The concentration of the hydrogen peroxide solution was exactly determined spectrophotometrically at $\lambda = 240$ nm before adding the catalase solution ($t = 0$). The time-dependent decrease (experiment time = 10 min) of absorption of hydrogen peroxide at $\lambda = 240$ nm ($\epsilon = 30 \text{ cm}^{-1}\text{M}^{-1}$) provided the value of the enzymatic activity. The activity number of the enzyme was calculated to $[\text{n}(\text{H}_2\text{O}_2) \times \text{min}^{-1}] / [\text{n}(\text{catalase})] = 2 \times 10^6$ (S4).

(b) Reactions in H₂O or D₂O with DMPO – differentiation of [•]OH from ¹O₂: To a solution of the dihydroxo complex **3** (200 μl, 5 × 10⁻³ mol/l) in H₂O or D₂O was added DMPO (200 μl, 0.18 mol/l) and then the mixture was irradiated (300 W halogen lamp, 1cm Perspex filter) in a screw cap NMR tube for 16 hrs under an atmosphere of nitrogen. 100 μl of the reaction mixture were transferred to an EPR flat cell and the spectrum was recorded. Experimental conditions: microwave power 20 mW, modulation amplitude 1 G, temperature 293 K. Both EPR spectra show the typical quartet for the DMPO-OH spin adduct (1 : 2 : 2 : 1, a_N = a_H = 14.9 G, (S7), Fig. S5a) in nearly the same intensity. If singlet oxygen is involved, the EPR signal in D₂O should have a five to ten times higher intensity compared to the signal measured in H₂O (S11).

(c) Reaction in H₂O with tetramethylpiperidine (TEMP) – differentiation between [•]OH and ¹O₂: To a solution of the dihydroxo complex **3** (200 μl, 5 × 10⁻³ mol/l) in H₂O was added a solution of TEMP (200 μl, 0.2 mol/l) in water and then the mixture was irradiated. The irradiation procedure, the volume of the EPR sample in the flat cell and the experimental conditions for the EPR experiment were the same as described in (b). No EPR signal was observed. If singlet oxygen would have been liberated, the tetramethylpiperidine-N-oxide (TEMPO) would be formed, giving a characteristic triplet EPR spectrum, a_N = 15.7 G (S12).

(d) Reactions in H₂O with DMPO/DMSO – confirmation of [•]OH radicals: To a solution of the dihydroxo complex **3** (200 μl, 5 × 10⁻³ mol/l) in H₂O was added DMPO (200 μl, 0.18 mol/l) and dimethylsulfoxide (DMSO) (various amounts between 10 μl and 30 μl, pure) and then the mixture was irradiated. The irradiation procedure, the volume of the EPR sample in the flat cell, and the experimental conditions for the EPR experiment were the

same as described in (b). We observed the characteristic sextet spectrum ($a_N = 15.5$ G, $a_H = 22.6$ G) with different intensities correlating with the concentration of DMSO (Fig. S5b). DMSO reacts with the liberated hydroxyl radicals to form carbon centred $\cdot\text{CH}_3$ -radicals. These methyl radicals react with DMPO to give the DMPO-CH₃ spin adduct producing the sextet EPR spectrum (S9).

(e) Irradiation of the hydrido-hydroxo complex ($2.nH_2O$) in H_2O with DMPO: To a solution of the hydrido-hydroxo complex ($2.nH_2O$) (200 μl , 5×10^{-3} mol/l) in H_2O was added DMPO (200 μl , 0.18 mol/l) and then the mixture was irradiated. The irradiation procedure, the volume of the EPR sample in the flat cell and the experimental conditions for the EPR experiment were the same as described in (b). No quartet was detected in the EPR spectrum, indicating that no OH radicals were liberated from $2.nH_2O$.

(f) Reactions in H_2O with DMPO and Catalase: To a solution of the dihydroxo complex **3** (200 μl , 5×10^{-3} mol/l) in H_2O was added DMPO (200 μl , 0.18 mol/l) as well as an aqueous catalase solution (100 μl , various concentrations between 5×10^{-7} mol/l and 5×10^{-18} mol/l) and then the mixture was irradiated. The irradiation procedure, the volume of the EPR sample in the flat cell and the experimental conditions for the EPR experiment were the same as described in (b). The EPR spectra show the typical quartet for the DMPO-OH spin adduct (1 : 2 : 2 : 1, $a_N = a_H = 14.9$ G, (S7), but the intensity of the quartet decreases with increasing concentration of enzyme. If the concentration of the enzyme is lower than 9×10^{-13} mol/l only a very modest quartet in the EPR spectra (Fig. S5c) was detected, implicating that the OH-radicals originate from hydrogen peroxide (S7).

TDDFT Calculations

UV-Vis Spectrum of a model of *cis*-(PNN)Ru(CO)(OH)₂ (^tBu and Et groups replaced by Me groups), **3***

The UV-VIS spectrum of this complex was determined in water by TDDFT at the M06/aug-SDB-cc-pVDZ//M06/SDD level of theory; for computational tractability, the phosphine and amine substituents were replaced by methyl groups, and this complex is denoted **3***. In the TDDFT calculation, ten singlet and ten triplet excitations were considered. The calculated spectrum of the model system is provided in Fig. S8.

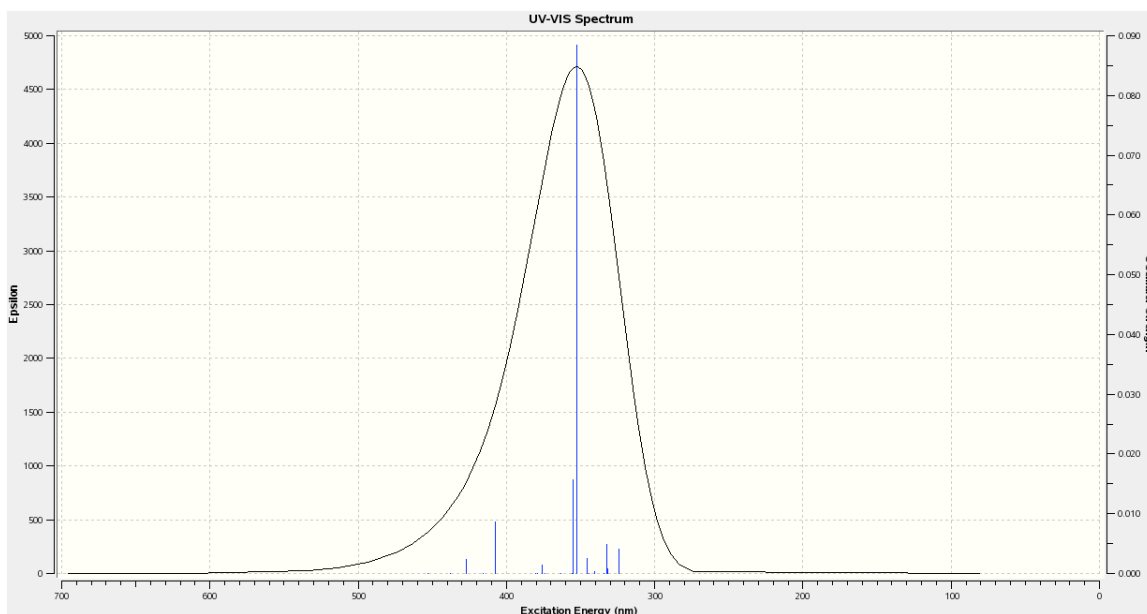


Fig. S8. Theoretical UV-Vis spectrum of *cis*-(PNN)Ru(CO)(OH)₂ **3*** as determined by TDDFT.

The main signal in the computed spectrum is at 352.57 nm with a contribution from a signal at 355.34 nm; this likely corresponds to the signal at 379.80 nm in the experimental spectrum (Fig. S2); Table S4 gives details of these excitations and selected molecular orbitals (MOs) are depicted in Fig. S9. In the computed spectrum, the main signal

corresponds primarily to an excitation from MO79 to MO82 while the minor signal corresponds to an excitation from MO81 to MO84. In both cases, this corresponds to a MLCT excitation from the Ru centre (with contributions from the OH and CO ligands) to the pyridine ring.

Table S4. TDDFT excitation energies around 350 nm for *cis*-(PNN)Ru(CO)(OH)₂ **3***

Shown are only the primary components of each excitation. The MOs are depicted in Fig. S9.

Excitation	From MO	To MO	Energy (eV)	Wavelength (nm)	Oscillator Strength
12	81	84	3.4892	355.34	0.0157
13	79	82	3.5166	352.57	0.0884

The experimental peak at 297.30 nm cannot be assigned at this time as insufficient excitations were considered.

The experimental peak at 459.31 nm is harder to assign as the computed spectrum does not have an obvious signal in this region. There are, however, a number of nearby singlet excitations with small oscillator strengths. In addition, a triplet excitation is possible due to the presence of a Ru atom. If one were to neglect relativistic effects, as is done in the TDDFT calculations, then triplet excitations are symmetry forbidden and thus TDDFT predicts 0.0000 oscillator strengths. However, if relativistic effects (specifically, spin-orbit coupling) are considered, than these “forbidden” excitations may have non-negligible oscillator strengths. That being said, determining these values is not trivial, especially for such large systems. Table S5 shows the calculated excitations in the region near 460 nm.

The triplet excitation at 452.79 nm (Excitation 1, MO81 to MO93) is likely best described as a *d-d* excitation. The triplet excitation at 438.01 nm and the singlet excitation at 427.32 nm are both HOMO-LUMO excitations of the MLCT type; the fourth excitation is MLCT excitation of the same kin as Excitation 13. The fifth excitation is similar to the first.

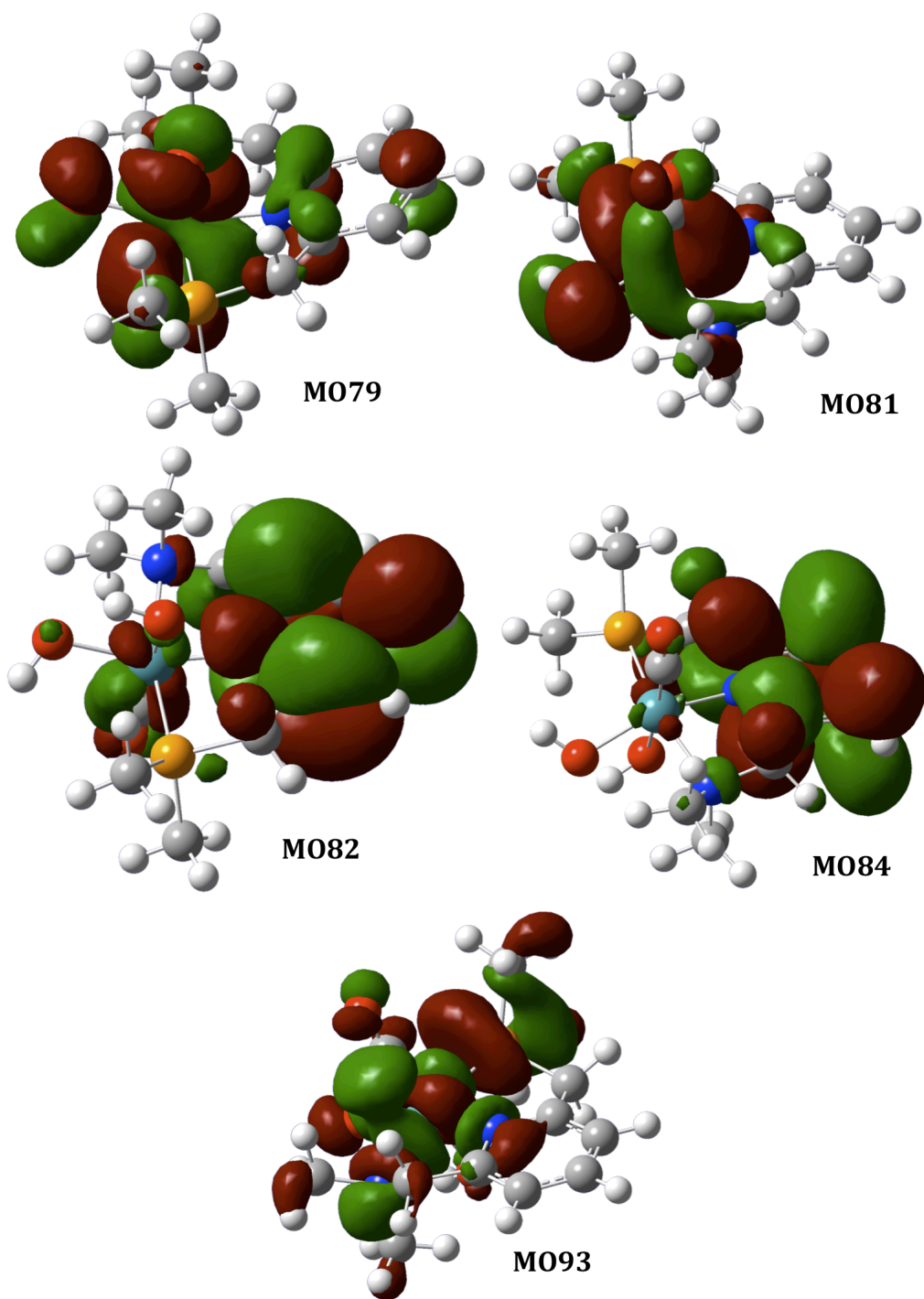


Fig. S9. Selected MOs of *cis*-(PNN)Ru(CO)(OH)₂ **3***

Table S5. TDDFT excitation energies around 460 nm for *cis*-(PNN)Ru(CO)(OH)₂. Shown are only the primary components of each excitation. The MOs are depicted in Figure S9.

Excitation	From MO	To MO	Energy (eV)	Wavelength (nm)	Oscillator Strength
1 (triplet)	81	93	2.7382	452.79	0.0000
2 (triplet)	81	82	2.8306	438.01	0.0000
3 (singlet)	81	82	2.9014	427.32	0.0023
4 (triplet)	79	82	2.9815	415.84	0.0000
5 (singlet)	81	93	3.0421	407.56	0.0086

Computational Methods

All calculations were carried out using Gaussian 03 Revision E.01 (S14), locally modified with the MNGFM patch (S15); this patch from the University of Minnesota adds the M06 (*vide infra*) family of DFT exchange-correlation functionals to the commercial version. The Minnesota06 (M06) hybrid meta-GGA DFT functional was used (S16). This functional has been shown to yield more reliable geometries, energies and reaction barrier heights for transition metal compounds than other “conventional” exchange-correlation functionals (S16, S17).

Four basis set-RECP (relativistic effective core potential) combinations were used. The first, denoted SDD, is the combination of the Huzinaga-Dunning double- ζ basis set (S18) on lighter elements with the Stuttgart-Dresden basis set-RECP combination (S19) on transition metals. The second, denoted SDD(d) is the same as SDD but with an additional

polarization function (i.e., the D95(d) basis set) on P and S atoms. The third, denoted SDB-cc-pVDZ, combines the Dunning cc-pVDZ basis set (S20) on the main group elements, and the Stuttgart-Dresden basis set-RECP (S19) on the transition metals with an added *f*-type polarization exponent taken as the average of the two *f*-exponents given in the appendix of reference (S21). The fourth is denoted as aug-SDB-cc-pVDZ and is the same as the previous but with the set of diffuse *spdf* functions from reference (S22) on the transition metals and Dunning's aug-cc-pVDZ basis set (S20) on the main group elements. In the simulation of the UV-Vis spectrum of *cis*-(PNN)Ru(CO)(OH)₂, the geometry was optimized using the SDD basis set and the TDDFT (electronic absorption spectrum) calculations were calculated with the aug-SDB-cc-pVDZ basis set. For studying the reactivity of **1** with water, the geometries were optimized with the SDD(d) basis set while the energetics of the reaction were evaluated with the SDB-cc-pVDZ basis set. The accuracy of the DFT method was improved by adding an empirical dispersion correction as recommended by Grimme (S23, S24). This is a correction that is added to the final energy and is a function of the geometry of the final, optimized geometry. Briefly, the dispersion energy is equal to (S23, S24):

$$E_{disp} = -s_6 \sum_{i=1}^{N_{at}-1} \sum_{j=i+1}^{N_{at}} \frac{C_6^{ij}}{R_{ij}^6} f_{dmp}(R_{ij})$$

$$f_{dmp}(R_{ij}) = \left(1 + \exp \left(-d \left(\frac{R_{ij}}{R_r} - 1 \right) \right) \right)^{-1}$$

$$C_6^{ij} = \sqrt{C_6^i C_6^j}$$

where R_r is the sum of van der Waal radii (r_{vdW}) of the two atoms in question and C_6^i is an empirical constant; these values for H-Xe have been determined by Grimme (S25). The s_6

is an empirical scaling factor unique for each DFT functional. For M06, it has been determined to be 0.25 (S26).

The r_{vdW} and C_6^i values are missing for the third-row transition metals (i.e., the entire sixth row of the periodic table). These values for the first and second row transition metals were determined by Grimme by averaging the values for the Groups 2 and 13 elements of the same row (S25). Thus, the r_{vdW} and C_6^i parameters for the third row transition metals were determined by averaging the parameters for Ba and Tl; the lanthanides were assigned parameters in the same manner. The parameters for these two elements, as well as the rest of the sixth row of the periodic table, were determined by a geometric extrapolation of the parameters for the preceding two rows.

The electronic spectra were simulated by using time dependent density functional theory (TDDFT) (S27-S29). In the TDDFT calculations, bulk solvent (water) effects were approximated using a polarizable continuum model (PCM),(S30-S33) specifically the integral equation formalism model (IEF-PCM) (S30, S31, S34, S35). In the TDDFT calculations, ten singlet and ten triplet excitations were considered.

References

- S1. J. Zhang, G. Leitun, Y. Ben-David, D. Milstein, *J. Am. Chem. Soc.* **127**, 10840-10841 (2005).
- S2. N. Ahmad, J. J. Levison, S. D. Robinson, M. F. Uttley, *Inorg. Synth.* **15**, 45-64 (1974).
- S3. A. L. Casalnuovo, J. C. Calabrese, D. Milstein, *J. Am. Chem. Soc.* **110**, 6738-6744 (1988).

- S4. R. F. Beers Jr., I. W. Sizer, *J. Biol. Chem.* 133-140 (1951).
- S5. O. Blum, D. Milstein, *J. Am. Chem. Soc.* **124**, 11456-11467 (2002).
- S6. P. Emsley, K. Cowtan, *Acta Cryst.* **D60**, 2126-2132 (2004).
- S7. B. E. Britigan, M. S. Cohen, G. M. Rosen, *J. Leukoc. Biol.* **41**, 349-362 (1987).
- S8. E. Finkelstein, G. M. Rosen, E. J. Rauckman, *Mol. Pharmacol.* **16**, 676-685 (1979).
- S9. L. M. Weiner, *Methods in Enzymology* **233**, 92-105 (1994).
- S10. P. Bilski, K. Reszka, M. Bilaska, C. F. Chignell, *J. Am. Chem. Soc.* **118**, 1330-1338 (1996).
- S11. E. Yavin, L. Weiner, R. Arad-Yellin, A. Shanzer, *J. Phys. Chem. A* **105**, 8018-8024 (2001).
- S12. L. E. Moan, E. Wold, *Nature* **279**, 450-451 (1979).
- S13. E. Ben-Ari, G. Leitun, L. J. W. Shimon, D. Milstein, *J. Am. Chem. Soc.* **128**, 15390-15391 (2006).
- S14. Gaussian 03, Revision E.01, M. J. Frisch, G. W. Trucks, H. B. Schlegel, G. E. Scuseria, M. A. Robb, J. R. Cheeseman, J. A. Montgomery, Jr., T. Vreven, K. N. Kudin, J. C. Burant, J. M. Millam, S. S. Iyengar, J. Tomasi, V. Barone, B. Mennucci, M. Cossi, G. Scalmani, N. Rega, G. A. Petersson, H. Nakatsuji, M. Hada, M. Ehara, K. Toyota, R. Fukuda, J. Hasegawa, M. Ishida, T. Nakajima, Y. Honda, O. Kitao, H. Nakai, M. Klene, X. Li, J. E. Knox, H. P. Hratchian, J. B. Cross, V. Bakken, C. Adamo, J. Jaramillo, R. Gomperts, R. E. Stratmann, O. Yazyev, A. J. Austin, R. Cammi, C. Pomelli, J. W. Ochterski, P. Y. Ayala, K. Morokuma, G. A. Voth, P. Salvador, J. J. Dannenberg, V. G. Zakrzewski, S.

- Dapprich, A. D. Daniels, M. C. Strain, O. Farkas, D. K. Malick, A. D. Rabuck, K. Raghavachari, J. B. Foresman, J. V. Ortiz, Q. Cui, A. G. Baboul, S. Clifford, J. Cioslowski, B. B. Stefanov, G. Liu, A. Liashenko, P. Piskorz, I. Komaromi, R. L. Martin, D. J. Fox, T. Keith, M. A. Al-Laham, C. Y. Peng, A. Nanayakkara, M. Challacombe, P. M. W. Gill, B. Johnson, W. Chen, M. W. Wong, C. Gonzalez, and J. A. Pople, Gaussian, Inc., Wallingford CT, 2004.
- S15. Minnesota Gaussian Functional Module version 3.1, Y. Zhao and D. G. Truhlar with assistance from M. A. Iron and J. M. L. Martin, University of Minnesota, Minneapolis, MN, 2008.
- S16. Y. Zhao, D. G. Truhlar, *Theor. Chem. Acc.* **120**, 215-241 (2008).
- S17. Y. Zhao, D. G. Truhlar, *Acc. Chem. Res.* **41**, 157-167 (2008).
- S18. T. H. Dunning Jr., P. J. Hay, *Modern Theoretical Chemistry*. H. F. S. III, Ed., (Plenum, New York, 1976), vol. 3, pp. 1-28.
- S19. M. Dolg, *Effective Core Potentials. In Modern Methods and Algorithms of Quantum Chemistry*. J. Grotendorst, Ed., (John von Neumann Institute for Computing, Jülich, 2000), vol. 1, pp. 479-508.
- S20. T. H. Dunning Jr., *J. Chem. Phys.* **90**, 1007-1023 (1989).
- S21. J. M. L. Martin, A. Sundermann, *J. Chem. Phys.* **114**, 3408-3420 (2001).
- S22. M. A. Iron, A. C. B. Lucassen, H. Cohen, M. E. van der Boom, J. M. L. Martin, *J. Am. Chem. Soc.* **126**, 11699-11710 (2004).
- S23. T. Schwabe, S. Grimme, *Phys. Chem. Chem. Phys.* **9**, 3397-3406 (2007).
- S24. T. Schwabe, S. Grimme, *Acc. Chem. Res.* **41**, 569-579 (2008).
- S25. S. Grimme, *J. Comput. Chem.* **27**, 1787-1799 (2006).

- S26. A. Karton, A. Tarnopolsky, J-F. Lamère, G. C. Schatz, and J. M. L. Martin, *J. Phys. Chem. A* **112**, 12868-12886 (2008).
- S27. R. Bauernschmitt, R. Ahlrichs, *Chem. Phys. Lett.* **256**, 454-464 (1996).
- S28. R. E. Stratmann, G. E. Scuseria, M. J. Frisch, *J. Chem. Phys.* **109**, 8128-8224 (1998).
- S29. M. E. Casida, C. Jamorski, K. C. Casida, D. R. Salahub, *J. Chem. Phys.* **108**, 4439-4449 (1998).
- S30. B. Mennucci, J. Tomasi, *J. Chem. Phys.* **106**, 5151-5158 (1997).
- S31. E. Cancès, B. Mennucci, J. Tomasi, *J. Chem. Phys.* **107**, 3032-3041 (1997).
- S32. M. Cossi, V. Barone, B. Mennucci, J. Tomasi, *Chem. Phys. Lett.* **286**, 253-260 (1998).
- S33. M. Cossi, G. Scalmani, N. Rega, V. Barone, *J. Chem. Phys.* **117**, 43-54 (2002).
- S34. B. Mennucci, E. Cancès, J. Tomasi, *J. Phys. Chem. B* **101**, 10506-10517 (1997).
- S35. J. Tomasi, B. Mennucci, E. Cancès, *J. Mol. Struct. (THEOCHEM)* **464**, 211-226 (1999).